



Repositorio Institucional de la Universidad Autónoma de Madrid

<https://repositorio.uam.es>

Esta es la **versión de autor** del artículo publicado en:

This is an **author produced version** of a paper published in:

Journal of Neuroscience 38.22 (2018): 5096-5110

DOI: <http://doi.org/10.1523/JNEUROSCI.3364-17.2018>

Copyright: © 2018 The Authors

El acceso a la versión del editor puede requerir la suscripción del recurso

Access to the published version may require subscription

Research Articles: Cellular/Molecular

R-Ras1 and R-Ras2 are essential for oligodendrocyte differentiation and survival for correct myelination in the central nervous system

Miriam Sanz-Rodríguez¹, Agnès Gruart³, Juan Escudero-Ramírez¹, Fernando de Castro², José María Delgado-García³, Francisco Wandosell¹ and Beatriz Cubelos¹

¹*Departamento de Biología Molecular and Centro Biología Molecular "Severo Ochoa", Universidad Autónoma de Madrid - Consejo Superior de Investigaciones Científicas, 28049 Madrid, Spain*

²*Instituto Cajal-CSIC, 28002 Madrid, Spain*

³*Division of Neurosciences, Pablo de Olavide University, 41013 Seville, Spain.*

DOI: 10.1523/JNEUROSCI.3364-17.2018

Received: 28 November 2017

Revised: 14 March 2018

Accepted: 10 April 2018

Published: 2 May 2018

Author contributions: M.S.-R., A.G., J.M.D.-G., and B.C. designed research; M.S.-R., A.G., J.E.-R., J.M.D.-G., and B.C. performed research; A.G., J.M.D.-G., F.W., and B.C. contributed unpublished reagents/analytic tools; M.S.-R., A.G., F.d.C., J.M.D.-G., F.W., and B.C. analyzed data; M.S.-R., A.G., J.M.D.-G., F.W., and B.C. wrote the paper.

Conflict of Interest: The authors declare no competing financial interests.

This work was supported by the Spanish Ministry of Economy and Competitiveness (BFU2015-64829-S and SAF2012-31279) to B.C. and (SAF2015-70368-R) to F.W. Authors wish to thank Drs. M. Izquierdo, P. Bovolenta, and B. Alarcón for helpful scientific discussions. We also want to thank Dr. A. Morales for providing us with the Nkx2.2 antibody, J.R. Perea, S. Gutierrez-Erlandsson, M. Guerra and T. Martin for their technical assistance, M. Sefton for critical reading of the manuscript and Life Science Editors for their editing assistance. The qPCR experimental development and data analysis was provided by the Genomics and NGS Core Facility at the Centro de Biología Molecular "Severo Ochoa", Madrid, Spain.

Corresponding author: Beatriz Cubelos PhD., Departamento de Biología Molecular. Centro de Biología Molecular Severo Ochoa, Nicolás Cabrera 1, Universidad Autónoma de Madrid, 28049 Madrid, Spain. Tel: 34-91-1964561; Fax: 34-91-1964420, Email: bcubelos@cbm.csic.es

Cite as: J. Neurosci ; 10.1523/JNEUROSCI.3364-17.2018

Alerts: Sign up at www.jneurosci.org/cgi/alerts to receive customized email alerts when the fully formatted version of this article is published.

The Journal of Neuroscience
 Regular article
 Cellular/Molecular
 Editors: David J. Perkel
 Anne Baron-Van Evercooren

Total number of pages: 44
 Total number of figures: 8
 Total number of words in the Abstract: 210
 Total number of words in the Significance Statement: 92
 Total number of words in the Introduction: 701
 Total number of words in the Discussion: 1155

R-Ras1 and R-Ras2 are essential for oligodendrocyte differentiation and survival for correct myelination in the central nervous system

Miriam Sanz-Rodriguez¹, Agnès Gruart³, Juan Escudero-Ramirez¹, Fernando de Castro², José María Delgado-García³, Francisco Wandosell¹ and Beatriz Cubelos^{1*}

¹Departamento de Biología Molecular and Centro Biología Molecular “Severo Ochoa”, Universidad Autónoma de Madrid - Consejo Superior de Investigaciones Científicas, 28049 Madrid, Spain; ²Instituto Cajal-CSIC, 28002 Madrid, Spain; ³Division of Neurosciences, Pablo de Olavide University, 41013 Seville, Spain.

Abbreviated title: Essential role of R-Ras1 and 2 in CNS myelination

Conflict of interest: Authors declare no conflict of interest

Acknowledgements: This work was supported by the Spanish Ministry of Economy and Competitiveness (BFU2015-64829-S and SAF2012-31279) to B.C. and (SAF2015-70368-R) to F.W. Authors wish to thank Drs. M. Izquierdo, P. Bovolenta, and B. Alarcón for helpful scientific discussions. We also want to thank Dr. A. Morales for providing us with the Nkx2.2 antibody, J.R. Perea, S. Gutierrez-Erlandsson, M. Guerra and T. Martin for their technical assistance, M. Sefton for critical reading of the manuscript and Life Science Editors for their editing assistance. The qPCR experimental development and data analysis was provided by the Genomics and NGS Core Facility at the Centro de Biología Molecular “Severo Ochoa”, Madrid, Spain.

*** Corresponding author:**

Beatriz Cubelos PhD,
 Departamento de Biología Molecular. Centro de Biología Molecular Severo Ochoa,
 Nicolás Cabrera 1, Universidad Autónoma de Madrid, 28049 Madrid, Spain.
 Tel: 34-91-1964561; Fax: 34-91-1964420
 Email: bcubelos@cbm.csic.es

45 **Abstract**

46 Rapid and effective neural transmission of information requires correct axonal
47 myelination. Modifications in myelination alter axonal capacity to transmit electric
48 impulses and enable pathological conditions. In the central nervous system (CNS),
49 oligodendrocytes (OLs) myelinate axons, a complex process involving various cellular
50 interactions. However, we know little about the mechanisms that orchestrate correct
51 myelination. Here, we demonstrate that OLs express R-Ras1 and R-Ras2. Using female
52 and male mutant mice to delete these proteins, we find that activation of the PI3K/Akt
53 and Erk1/2-MAPK pathways is weaker in mice lacking one or both of these GTPases,
54 suggesting that both proteins coordinate the activity these two pathways. Loss of R-
55 Ras1 and/or R-Ras2 diminishes the number of OLs in major myelinated CNS tracts and
56 increases the proportion of immature OLs. In *R-Ras1^{-/-}* and *R-Ras2^{-/-}* null mice, OLs
57 show aberrant morphologies and fail to differentiate correctly into myelin-forming
58 phenotypes. The smaller OL population and abnormal OL maturation induce severe
59 hypomyelination, with shorter nodes of Ranvier in *R-Ras1^{-/-}* and/or *R-Ras2^{-/-}* mice.
60 These defects explain the slower conduction velocity of myelinated axons we observed
61 in the absence of R-Ras1 and R-Ras2. Together, these results suggest that R-Ras1 and
62 R-Ras2 are upstream elements that regulate the survival and differentiation of
63 progenitors into OLs through the PI3K/Akt and Erk1/2-MAPK pathways for proper
64 myelination.

65

66 **Significance Statement**

67 In this study, we show that R-Ras1 and R-Ras2 play essential roles in regulating
68 myelination *in vivo* and control fundamental aspects of oligodendrocyte survival and
69 differentiation through synergistic activation of PI3K/Akt and Erk1/2-MAPK signaling.
70 Mice lacking R-Ras1 and/or R-Ras2 show a diminished oligodendrocyte population
71 with a higher proportion of immature oligodendrocytes, explaining the observed
72 hypomyelination in main CNS tracts. *In vivo* electrophysiology recordings demonstrate
73 a slower conduction velocity of nerve impulses in the absence of R-Ras1 and R-Ras2.
74 Thus, R-Ras1 and R-Ras2 are essential for proper axonal myelination and accurate
75 neural transmission.

76

77 **Introduction**

78 Mammalian plasma membranes from specialized glial cells generate myelin as
79 oligodendrocytes in the central nervous system and Schwann cells in the peripheral
80 nervous system. Axonal myelination is essential to facilitate fast, saltatory conduction
81 of action potentials. Changes in myelin structure, such as sheath thickness and internode
82 length, can alter axonal conduction velocities, which may induce pathologies like
83 leukodystrophies and peripheral neuropathies (Suter and Scherer, 2003; Boespflug-
84 Tanguy et al., 2008).

85 During development, oligodendrocyte progenitor cells (OPCs), which differentiate into
86 OLs, arise along the caudorostral axis of the ventricular neuro-epithelium of the neural
87 tube at multiple restricted foci distributed along the dorsoventral axis to colonize the
88 entire CNS (de Castro F., 2013; Ono et al., 2017). OPCs then differentiate into mature
89 OLs forming myelin (Nave and Werner, 2014). Various intrinsic and extrinsic cues, like
90 specific growth factors, protein kinases and extracellular matrix proteins regulate the
91 spatial and temporal patterns of OL differentiation by modifying gene expression and
92 cell morphology (Bauer et al., 2009; Emery, 2010).

93 Among these factors, PI3K/Akt and Erk1/2-MAPK signaling pathways may control OL
94 survival, migration, differentiation and myelination (Ness et al., 2002; Romanelli et al.,
95 2009; Ishii et al., 2014; Murcia-Belmonte et al., 2014; Gaesser and Fyffe-Maricich,
96 2016; Murcia-Belmonte et al., 2016). Indeed, mutant animals that have constitutively-
97 active PI3K-Akt-mTOR pathways in their OPCs and OLs show dramatically enhanced
98 myelin formation but not changes in OL generation (Flores et al., 2008; Goebbels et al.,
99 2010; Harrington et al., 2010). In contrast, inhibition of effectors of the PI3K/Akt
100 pathway such as mTOR causes defective OL differentiation both *in vitro* and *in vivo*
101 (Tyler et al., 2009; Wahl et al., 2014). Erk1/2 signaling controls thickness and

102 maintenance of CNS myelin (Wahl et al., 2014; Ishii 2014), and its inactivation produces
 103 a delay in the differentiation and maturation of OLs (Fyffe-Maricich et al., 2011).
 104 Hyperactivation of the Erk1/2-MAPK pathway during development drives a transient
 105 OPC hyperproliferation without affecting their differentiation or the final number of
 106 mature OLs (Ishii et al., 2013). In addition, Erk1/2 activation in OLs drives sheath
 107 expansion (Jeffries et al., 2016) (Jeffries et al., 2016). It is known that there is cross-talk
 108 between PI3K/Akt and Erk1/2-MAPK (Gaesser and Fyffe-Maricich, 2016; Furusho et
 109 al., 2017), though little is known about the mechanisms that mediate the coordinated
 110 activity of signaling in these two molecular pathways.

111 One candidate is the Ras superfamily of GTP-binding proteins. These membrane-
 112 anchored intracellular signal transducers that act through both PI3K/Akt and Erk1/2-
 113 MAPK pathways (Arimura and Kaibuchi, 2007) to influence various cell functions,
 114 including proliferation, differentiation and cell survival (Karnoub and Weinberg, 2008;
 115 Pylayeva-Gupta et al., 2011). Members of the classic Ras subfamily (*Hras*, *Kras* and
 116 *Nras*) are frequently mutated and constitutively active in human cancers (Chan et al.,
 117 1994). GTPases of the Ras-related (R-Ras) subfamily, composed of *R-RAS1* (*RRas*), *R-*
 118 *RAS2* (*TC21*) and *R-RAS3* (also called *MRas*), are less well understood (Ohba et al.,
 119 2000; Colicelli, 2004; Gutierrez-Erlandsson et al., 2013). R-Ras proteins share strong
 120 homology (55-60% amino acid identity) with classic Ras proteins (Drivas et al., 1990;
 121 Colicelli, 2004), and with many effector proteins, including components in PI3K/Akt
 122 and Erk1/2-MAPK pathways (Chan et al., 1994; Graham et al., 1994; Graham et al.,
 123 1999; Movilla et al., 1999; Rosario et al., 1999, 2001; Delgado et al., 2009). R-Ras1 and
 124 R-Ras2 are almost ubiquitously expressed (Komatsu and Ruoslahti, 2005; Larive et al.,
 125 2012), whereas R-Ras3 expression is more restricted (Kimmelman et al., 2002; Sun et
 126 al., 2006). In the CNS, OLs can express R-Ras1 (Olsen and French-Constant, 2005),

127 however its specific function and putative role with R-Ras2 in myelination remains
128 unknown.

129 Here we investigated the role of R-Ras1 and R-Ras2 in OL differentiation for myelin
130 formation, using three knockout mice: (single *R-Ras1* or *R-Ras2* null mutants, and a
131 double null mutant). Different levels of hypomyelination in *R-Ras1*^{-/-} and *R-Ras2*^{-/-} mice
132 indicate that both GTPases are essential for proper myelination. Single and double null
133 mutant mice showed diminished OL viability from weaker activation of PI3K/Akt and
134 Erk1/2-MAPK signaling. OL maturation was altered, changing the internode length
135 (myelin segments between nodes of Ranvier), which strongly decreased axonal
136 conduction velocity. Overall, our data strongly suggest that R-Ras1 and R-Ras2 are
137 critical for OL differentiation and CNS myelination through mechanisms using Akt and
138 Erk pathways.

139 **Material and Methods**

140 *Animals.* Mice were housed in specific pathogen-free conditions, in a humidity and
141 temperature-controlled room on a 12-h light/dark cycle, receiving water and food *ad*
142 *libitum*. All animal procedures were approved by the corresponding institutional ethical
143 committee (CBMSO) and were performed in accordance with Spanish and European
144 directives. All efforts were made to minimize animal suffering.

145 *R-Ras1*^{-/-} mice were generated at GenoWay Company (France) using the targeting
146 construction BAL1-HR with a neomycin resistance cassette flanked by FRT sequences
147 inserted in intron 1 and LoxP sites flanking exons 2 and 6. The construction was
148 electroporated into embryonic stem cells derived from mouse 129Sv/Pas and selected
149 by the antibiotic G418. Southern blot was used to verify the correct homologous
150 recombination.

151 Heterozygous mice were crossed, and offspring littermates were genotyped by PCR (*R-*
152 *Ras1*^{-/-} FW: 5'-GGAGCAAGAGGAGGGAAGGAATGGG-3', *R-Ras1*^{-/-} RV: 5'-
153 CCTTCCAGAGGACTCAGTTCAATCC-3', *R-Ras1*^{+/+} FW: 5'-
154 CGCTCTAGCTGAGCCTCTGT-3', *R-Ras1*^{+/+} RV: 5'-
155 TACAGGGTCTTGTGGGGAAA-3').

156 *R-Ras2*^{-/-} mice were generated at Lexicon Pharmaceuticals (Texas, USA) and were
157 derived from embryonic stem cell clone OST361011 with insertion of retroviral
158 VICTR37 in the middle of intron 1 of *R-Ras2*. Heterozygous mice were crossed and
159 offspring littermates were genotyped by PCR (primer 1, 5'-
160 TGAAACAGGATCATGTTGTGGAG-3'; primer 2, 5'-
161 CAGGAGGAGTCCAAGAAGAC-3'; primer 3, 5'-
162 ATAAACCCTCTTGCAGTTGCATC-3') (Delgado et al., 2009). *R-Ras2*^{+/+} and *R-*
163 *Ras2*^{-/-} transgenic mice were obtained by crossing of heterozygous mice.

164 *R-Ras1^{-/-}* and *R-Ras2^{-/-}* mice were kindly provided by Prof. Alarcón (CBMSO, Spain).
 165 Double-knockout *R-Ras1^{-/-};R-Ras2^{-/-}* mice were generated by backcrossing individual
 166 lines of *R-Ras1^{-/-}* and *R-Ras2^{-/-}*. Animals were maintained in a C57BL6J background.
 167 We have used either, male and female mice to perform the experiments. The morning
 168 the vaginal plug appeared was defined as embryonic day (E) 0.5, and newborn was
 169 defined as postnatal (P) 0.
 170 *Western blotting.* Tissue samples (optic nerve, spinal cord and corpus callosum of
 171 animals from P30 to P90) were dissected, sonicated in lysis buffer (50 mM Tris pH 8.0,
 172 150 mM NaCl, 1% NP40, 2 mM EDTA, 0.1% SDS, 0.5% desoxycholate, Protease
 173 Inhibition Cocktail; Roche 11697498001, Basel, Switzerland) and phenylmethane
 174 sulfonyl fluoride (PMSF). For detection of phosphorylated proteins, a different buffer
 175 was used (40 mM Tris pH 8.0, 300 mM NaCl, 20% Glycerol, 4 mM EDTA, 0.3% Brij
 176 96, 1 mM PMSF, 2 mM Na₃VO₄, 10 mM NaF, 1 mM apoprotein, 1 mM benzamidine, 1
 177 mM iodoacetamide, and protease inhibitor cocktail. Lysates were denatured by boiling
 178 for 5 min in protein loading buffer (50 mM Tris-HCl pH 6.8, 2% SDS, 10% glycerol,
 179 1% β-mercaptoethanol (BME), 12.5 mM EDTA and 0.02 % bromophenol blue) and
 180 resolved in 10-12% SDSP-gels in the presence of BME. Gels were run at constant
 181 current starting at 90-100V. After electrophoresis, samples were transferred onto PVDF
 182 membranes using a semi-dry electroblotting system (Transblot-turbo, BioRad,
 183 California, USA) at 1.2 mA/cm² for 35-40 min. Nonspecific protein binding was
 184 blocked by incubating the membrane with 5% non-fat milk or 5% BSA (for detection of
 185 phosphorylated proteins) in TBS-Tween-20 for 2 h at room temperature. Membranes
 186 were then incubated overnight at 4 °C with the pertinent primary antibodies diluted in
 187 blocking buffer: rabbit anti-R-Ras 1:200 (ab154962), rabbit anti-Caspr 1:250 (Abcam
 188 Cat# ab34151, RRID: AB_869934, Cambridge, UK), mouse anti-GAPDH (G9) 1:1000

189 (Santa Cruz Biotechnology Cat# sc-365062, RRID:AB_10847862, Dallas, Texas,
 190 USA), goat anti-MAG (C-19) 1:200 (Santa Cruz Biotechnology Cat# sc-9544,
 191 RRID:AB_670102), rabbit anti-Akt 1:1000 (Cell Signaling Technology Cat# 9272,
 192 RRID:AB_329827, Massachusetts, USA), rabbit anti-P-Akt (S473) 1:1000 (Cell
 193 Signaling Technology Cat# 4060, RRID:AB_2315049), rabbit anti-P-Akt (T308)
 194 1:1000 (Cell Signaling Technology #9275), rabbit anti-phospho S6 (S240/244) 1:1000
 195 (Cell Signaling Technology Cat# 5364, RRID:AB_10694233), rabbit anti-p44/42
 196 MAPK (Erk1/2) 1:1000 (Cell Signaling Technology Cat# 9102, RRID:AB_330744),
 197 rabbit anti-P-p44/42 MAPK (P-Erk1/2) (T202/T204) 1:1000 (Cell Signaling
 198 Technology Cat# 9101, RRID:AB_331646), mouse anti-MBP (aa67-74) 1:200 (Bio-
 199 Rad / AbD Serotec Cat# MCA685S, RRID:AB_325009, Raleigh, North Carolina,
 200 USA), mouse anti-TCF-4 clone 6H5-3 1:1000 (Millipore Cat#05-511,
 201 RRID:AB_309772, Missouri, USA) or rabbit anti-Olig2 1:2000 (Millipore Cat#
 202 AB9610, RRID:AB_570666). Specific rabbit antiserum to R-Ras2 (kindly provided by
 203 Prof B. Alarcón) was generated by immunization of New Zealand rabbits with a
 204 purified GST-TC21 fusion protein (Delgado et al., 2009), and used at a 1:200 dilution.
 205 After washing, blots were then incubated for 1 h with appropriate peroxidase-
 206 conjugated secondary antibodies (ThermoFisher, Waltham, Massachusetts, USA).
 207 Labeled proteins were detected with the chemiluminescence reagent ECL (Amersham
 208 Biosciences, USA).
 209 *Immunohistochemistry.* Animals were anesthetized (ketamine/xylazine) and perfused
 210 transcardially with 0.1 M phosphate-buffered saline (PBS; pH 7.4) followed by 4%
 211 paraformaldehyde in PBS. Perfused tissues were removed and postfixed in 4%
 212 paraformaldehyde at 4 °C overnight, then cryoprotected in 30% sucrose in PBS and
 213 embedded and frozen in a 7.5% gelatin in 15% sucrose solution. Then they were

214 sectioned on a cryostat to produce 15 μ M-thick cryosections on Superfrost Plus
 215 microscope slides (Fisher Scientific, Pittsburgh, PA, USA). Sections were blocked for 1
 216 h at room temperature with 10% fetal bovine serum in PBS containing 0.5% Triton-X
 217 100 (blocking solution) and then incubated overnight at 4 °C with the primary
 218 antibodies (rabbit anti-R-Ras 1:200, rabbit anti-R-Ras2 1:500, mouse anti-Nkx2.2 1:250
 219 (DSHB Cat# 74.5A5, RRID:AB_531794, Iowa, USA), kindly provided by Aixa
 220 Morales (Cajal Institute, CSIC, Madrid, Spain), rabbit anti-olig2 1:500, rabbit anti-
 221 cleaved caspase-3 (Asp175) 1:500 (Cell Signaling Technology Cat# 9661,
 222 RRID:AB_2341188), rabbit anti-MBP 1:300 (Abcam Cat# ab40390,
 223 RRID:AB_1141521), mouse anti-NF200 clone NE14 1:300 (Sigma-Aldrich Cat#
 224 N5389, RRID:AB_260781, St. Louis, Missouri, USA), rabbit anti-Caspr 1:250, mouse
 225 anti-TCF-4 clone 6H5-3 1:200 and mouse anti-O4 1:200 (Millipore Cat# MAB345,
 226 RRID:AB_94872) diluted in blocking solution. After 3 washes, fluorescent-tagged
 227 secondary antibodies were applied for 1 h at room temperature, and sections were
 228 counterstained with DAPI (32670, Sigma-Aldrich, St. Louis, MO, USA) and mounted
 229 in Aqua-polymount mounting medium (Cat#18606; Polyscience; Warrington, PA,
 230 USA).
 231 BrdU injections were administered intraperitoneally to pregnant mice (100 μ g/g) at
 232 different stages of embryo development. One hour after BrdU administration, the
 233 mother was euthanized and the brains of embryos were fixed overnight in 4% PFA.
 234 Staining for BrdU was performed as described (Cubelos et al., 2008). Briefly, slides
 235 were incubated overnight at 4 °C with a mouse monoclonal anti-BrdU antibody 1:200
 236 (Becton Dickinson Cat# 347580, RRID: AB_609568, New Jersey, USA). Secondary
 237 Alexa 598-conjugated anti-rat antibodies 1:500 (Molecular Probes, Eugene, Oregon,
 238 USA) were applied for 2 h at room temperature. Anatomically-matched sections were

239 selected from each mouse at each stage after BrdU injection (n=3, control mice
 240 and n=3, *R-Ras1*^{-/-}; *R-Ras2*^{-/-} mice). Identical results were obtained from independent
 241 analysis by two investigators. Quantification of positive cells was performed always in
 242 the same part of the tissues with ImageJ software (RRID:SCR_003070, Wisconsin-MA,
 243 USA).

244 *Toluidine blue staining.* Mice were anesthetized as indicated above, intracardially
 245 perfused with 4% PFA and 2.5% glutaraldehyde in 0.1 M PBS, and brains were
 246 dissected and treated in the same fixative overnight. Sections were made with a Leica
 247 VT1200 S vibrating blade microtome (100 µm), washed 10 min in PBS and stained for
 248 1 min with 200 µl of 0.1% toluidine blue, and finally washed with distilled water and
 249 ethanol for 30 sec. Pictures were taken with a Leica MZ6 magnifying glass for the
 250 proper location of implanted recording electrodes.

251 *Electron microscopy.* **Mutant** and littermate control mice were anesthetized as
 252 indicated above, intracardially perfused with 4% PFA and 2.5% glutaraldehyde in 0.1 M
 253 PBS, and treated in the same fixative overnight. Then, optic nerves were removed after
 254 several washes in PBS, the sections were postfixated with 1% osmium tetroxide in
 255 double-distilled water and 1% potassium ferrocyanide 1 h at 4 °C. After three washes
 256 with double-distilled water they were treated with 0.15% tannic acid in PBS (0.1 M pH
 257 7.4) and block-stained with 2% uranyl acetate in distilled water for 1 h at room
 258 temperature in darkness. Sections were then washed 3 times with double-distilled water
 259 and dehydrated in an ascending series of ethanol dilutions up to 100% at 4 °C. The
 260 following infiltration was made with propylene oxide: EtOH (1:1; v:v) for 5 min,
 261 propylene oxide 3 times for 15 min each, propylene oxide:Epon (1:1) (epoxy resin
 262 TAAB 812, TAAB laboratories, Berkshire, England) 45 min, 100% Epon 1 h, 100%
 263 Epon overnight. Encapsulation was made in flat molds where optic nerves were

264 correctly oriented and then polymerized 48 h at 60 °C. Semi-thin (1 μ m) sections were
 265 stained with toluidine blue. The optic nerve was cut in 70-80 nm sections on an
 266 ultramicrotome (Leica Ultracut UCT, Wetzlar, Germany) with a diamond blade
 267 (DIATOME) and collected on Cu-Pd boutonniere grids covered by Formvar. Staining
 268 of ultrathin sections was performed by drops of 2% aqueous uranyl acetate for 7 min
 269 followed by Reynolds's lead citrate for 2 min. Ultrastructural analyses were performed
 270 with a JEM-1010 electron microscope (Jeol, Japan). For g-ratio analysis, twelve
 271 pictures were taken along the section covering the whole diameter of the optic nerve
 272 using a CMOS 4K x 4K, F416 of TVIPS camera (Gauting, Germany). From these
 273 pictures, six in perfect condition that matched the mutant and control, were used to
 274 measure the thickness of the myelin sheath of optic nerve axons by g-ratio analysis (the
 275 diameter of axon / the diameter of axon plus myelin sheath). All axons present in the
 276 entire image were analyzed (around 800-1000 axons per genotype). To quantify the
 277 number of fibers crossing the *corpus callosum*, pictures were taken in the medial *corpus*
 278 *callosum* covering its whole width, and the total number of axons were quantified.
 279 Three animals per genotype were analyzed, and identical results were obtained from
 280 independent analysis by 3 investigators.

281 *Confocal microscopy and imaging.* Fluorescence images were obtained using a confocal
 282 multispectral Leica TCS SP8 system (Leica Microsystems) equipped with a white-light
 283 laser for selection of appropriate fluorochrome excitation lines (488 nm and 550 nm), a
 284 405 nm diode for DAPI excitation and HyD detectors for signal emission capture.
 285 Image acquisition was performed sequentially using 20x/0.75 NA dry and 63x/1.4NA
 286 oil immersion objectives with LAS X v. 2.0.1 software (Leica Microsystems). All
 287 images were processed and quantified using Adobe PhotoShop (Adobe Systems,
 288 RRID:SCR_014199, San Jose, CA, USA) and ImageJ.

289 *Primary cell cultures and staining.* OPCs were obtained from cortex and optic nerve of
 290 P1 control and *R-Ras1^{-/-};R-Ras2^{-/-}* littermate mice, following an adapted protocol for
 291 OPC isolation by shaking (McCarthy and de Vellis, 1980; Molina-Holgado et al., 2002;
 292 Medina-Rodriguez et al., 2013; Murcia-Belmonte et al., 2014).
 293 Purified OPCs were placed on 12 mm cover glass pre-treated with 10 µg/ml poly-lysine
 294 (#P2636; Sigma-Aldrich; St. Louis, MO, USA) in 0.1 M borate buffer (pH 8.5) and
 295 laminin (L2020; Sigma-Aldrich) the same day of the culture. 20000 cells per well were
 296 cultured in differentiation buffer containing BME (41010; Gibco; Grand Island, New
 297 York, USA), F12 (21765; Gibco), transferrin (T0665; Sigma-Aldrich), putrescine
 298 (P5780; Sigma-Aldrich), progesterone (P6149; Sigma-Aldrich), sodium selenite
 299 (Sigma-Aldrich), insulin (I1882; Sigma-Aldrich), T4 (T1775; Sigma-Aldrich),
 300 glutamine (25030; Gibco), anti-mycotic solution and 0.6% glucose. After 14 days *in*
 301 *vitro* (DIV) of differentiation, OLs were fixed with 4% PFA for 20 min and washed.
 302 OLs were placed in PBS containing 0.5% Triton-X 100 for 20 min and then blocking
 303 solution (10% FBS in PBS containing 0.5% Triton-X 100) for 30 min. After that, they
 304 were incubated for 2 h at room temperature with primary antibodies (1:500 dilution of
 305 mouse anti-CNPase, Biolegend, #SMI-91R, RRID: AB_10122287, St. Diego,
 306 California, USA or a 1:250 dilution of rabbit anti-Olig2). After washing, cells were
 307 incubated 35 min with fluorescent-tagged secondary antibodies and DAPI (32670;
 308 Sigma-Aldrich). OLs from three different experiments were classified according to their
 309 morphologies in two different groups (Kremer et al., 2009), one where the number and
 310 complexity of processes was very low (simple processes) and another where the
 311 processes had a high degree of arborization (complex processes).
 312 *RT-qPCR.* RNA was extracted from optic nerves from control, *R-Ras1^{-/-}*, *R-Ras2^{-/-}* and
 313 *R-Ras1^{-/-};R-Ras2^{-/-}* mice using an RNeasy kit according to the manufacturer's

314 instructions (Qiagen Cat# 74134; Venlo, Netherlands). RNA was reverse-transcribed
 315 using random hexamers and SuperscriptIII reverse transcriptase (Superscript III First
 316 Strand Synthesis Supermix for qRT-PCR, no amperase UNG, Cat. No. 11752-250,
 317 Thermofisher; Waltham, MA, USA) according to the manufacturer's instructions.
 318 cDNA was amplified using the BioRadC FX 384 thermocycler and Eva Green Sso Fast
 319 (BioRad, California, USA), Power Sybr Green or Taqman Master Mix. The following
 320 primers were used: For *R-Ras1* (R-Ras-FW sense 5'-
 321 AAGGCAGATCTGGAGAACCA-3', R-Ras-RV antisense 5'-
 322 TGCCTCATCGACATTCAGAC-3'), for *R-Ras2* (R-Ras2-FW sense 5'-
 323 CGTGATGAGTTTCCCATGATT-3', R-Ras2-RV antisense 5'-
 324 TAACTGCTGCCCTTCTTCCT-3'). All primers were designed to span at least one
 325 intron. Expression levels were normalized to GAPDH, ActB, HPRT1, 18S, TBP, ARBP
 326 and GUSB expression, and fold-changes were calculated by dividing normalized
 327 expression in control (value 1) by that of *R-Ras1*^{-/-} or *R-Ras2*^{-/-}. qPCR data was analyzed
 328 with GenEx Professional 5.3.7 software (MultiD, Sweden).
 329 *Electrophysiology.* Control (n=9), *R-Ras1*^{-/-} (n=13), *R-Ras2*^{-/-} (n=13) and *R-Ras1*^{-/-};*R-*
 330 *Ras2*^{-/-} (n=14) mice were prepared for chronic recording of field potentials evoked at the
 331 lateral geniculate nucleus by stimulus (flashes of light). For this, animals were
 332 anesthetized with 4% chloral hydrate and stereotaxically implanted with two recording
 333 electrodes in the dorsal part of the lateral geniculate nucleus (2.2-2.5 mm posterior to
 334 the bregma, 2.0 mm lateral to the midline and -2.5 mm depth from brain surface
 335 (Paxinos and Franklin, 2013). Electrodes were made from 50 µm teflon-coated tungsten
 336 wire (Advent Research Materials, Eynsham, UK). Two bare silver wires were affixed to
 337 the skull as ground. Electrodes were connected to a 4-pin socket (RS-Amidata, Madrid,
 338 Spain) that was latterly fixed with dental cement to the cranial bone. After surgery,

339 animals were kept for 5 days in independent cages with free access to food and water
340 for a proper recovery. Light stimulation was provided by a xenon arc lamp located 30
341 cm in front of the animals' eyes and lasted ~1 ms (Photic stimulator, Cibertec, Madrid,
342 Spain). For recordings, each alert behaving mouse was placed in a transparent box ($5 \times$
343 5×5 cm), dark-adapted for >30 min and presented with a total of 20 stimuli at a rate of
344 3 per min. This box was in the center of a larger ($30 \times 30 \times 30$ cm) covered by polished
345 aluminum walls. Photic stimulations were triggered from a programmable CS-20
346 stimulator (Cibertec). Each animal received two stimulation sessions.

347 *Statistical Analysis.* Quantitative data are presented as the mean \pm standard deviation
348 (SD). The experimental groups were compared using a two-tailed Student's t-test.
349 Statistical numeric data are provided in the legends. (*) means $p < 0.05$; (**) means
350 $p < 0.01$; (***) means $p < 0.001$.

351 **Results**

352 **R-Ras1 and R-Ras2 are expressed by oligodendrocytes in myelinated CNS tracts**

375 While OLs may express R-Ras1 (Olsen and Ffrench-Constant, 2005), the distribution of
 376 R-Ras2 remains undetermined. So, we precisely defined the expression of R-Ras1 and
 377 R-Ras2 in different myelinated areas of the CNS in adult mice (P90). Using
 378 immunoblotting, we probed samples from the main myelinated tracts of the CNS for R-
 379 Ras1 and R-Ras2, including: the optic nerve (which consists almost entirely of
 380 myelinated axons) (Fig. 1A), corpus callosum (Fig. 1B) and spinal cord (Fig. 1C). Given
 381 the strong homology between R-Ras1 and R-Ras2, antibodies against these GTPases
 382 recognize both proteins. We can easily detect two bands of different molecular weights
 383 in Western blots: a 25 kDa band corresponding to R-Ras1 (Iwasawa et al., 2012) and a
 384 21 kDa band corresponding to R-Ras2 (Delgado et al., 2009). In double null mutant
 385 mice lacking both R-Ras1 and R-Ras2, no immunoreactivity was observed, confirming
 386 the antibodies used are specific for R-Ras1 and R-Ras2 (Fig. 1A-C). We could
 387 unequivocally confirm the absence of the appropriate proteins in the single null mutants
 388 (Fig. 1A). R-Ras3 expression was not modified in *R-Ras1*^{-/-} and/or *R-Ras2*^{-/-} mice,
 389 showing a band of 24 kDa (Fig. 1A-C).

390 To generate R-Ras1 deletion mutants, we used a germ-line knockout mouse with exons
 391 2-6 deleted, the region that encodes most of the protein (Fig. 1D). We genotyped mice
 392 by PCR using primers 1 and 2 to detect the alleles corresponding to *R-Ras1*^{+/+} mice and
 393 a mixture of primers 3 and 4 to identify the *R-Ras1*^{-/-} mutants (Fig. 1E). We also used a
 394 R-Ras2 knockout mouse line produced from an embryonic stem cell clone with a
 395 retroviral insert in the first intron of R-Ras2 (Delgado et al., 2009) (Fig. 1F). Finally, we
 396 generated *R-Ras1/R-Ras2* double null mutant mice by backcrossing the individual *R-*
 397 *Ras1*^{-/-} and *R-Ras2*^{-/-} lines. These mice were backcrossed for ten generations onto the

398 C57BL/6J strain to exclude any distortions induced by background variations.
 399 Quantitative PCR and immunoblot analysis of the CNS confirmed the absence of
 400 expression of these genes in *R-Ras1^{-/-}*, *R-Ras2^{-/-}* and double-mutant mice (Fig.
 401 1A,B,C,G).

402 We then determined whether OLs express R-Ras1 and R-Ras2 using double
 403 immunohistochemical staining with antibodies against R-Ras1/R-Ras2 and Nkx2.2, a
 404 homeobox transcription factor expressed by oligodendroglial cells (Qi et al., 2001). In
 405 longitudinal sections of the optic nerve from adult mice (P90), both R-Ras1 and R-Ras2
 406 co-localized with Nkx2.2 (Fig. 1H), which was also observed in the corpus callosum
 407 and spinal cord (data not shown). So, we conclude that R-Ras1 and R-Ras2 are
 408 expressed in OLs of the main myelinated CNS tracts.

409 **Oligodendrocyte population is diminished in *R-Ras1^{-/-}*, *R-Ras2^{-/-}* and *R-Ras1^{-/-};R-*
 410 *Ras2^{-/-}* mice**

411 To study whether the absence of R-Ras1 and/or R-Ras2 altered oligodendroglial cells,
 412 we utilized immunohistochemical staining of optic nerves with the oligodendroglial-
 413 specific Olig2 antibody in longitudinal sections from *R-Ras1^{-/-}*, *R-Ras2^{-/-}* and double-
 414 mutant adult (P90) mice (Fig. 2A,B). Histological examination revealed a decrease in
 415 oligodendroglial cell density in *R-Ras1^{-/-}* (19.1±7.5% reduction; p=0.02), *R-Ras2^{-/-}*
 416 (33.5±2.1% reduction; p<0.0001) and *R-Ras1^{-/-};R-Ras2^{-/-}* (42.8±11.8% reduction;
 417 p=0.003) mice compared to controls (Fig. 2A,C). The reduction in oligodendroglial cells
 418 was more pronounced in double mutants (p=0.02) followed by *R-Ras2^{-/-}* (p=0.003)
 419 compared with *R-Ras1^{-/-}* (Fig. 2C). We examined whether R-Ras1 and R-Ras2 were
 420 essential to maintain the OL population in other myelinated CNS tracts and confirmed
 421 the reduction in oligodendroglial population in the double-mutant mice compared to
 422 controls (38±15.6% reduction in the corpus callosum, p<0.0001; and 27±6.1% reduction

423 in the spinal cord, $p=0.007$; data not shown). These observations demonstrate that R-
 424 Ras1 and R-Ras2 jointly maintain the OL populations in the main myelinated CNS
 425 tracts.

426 **Absence of R-Ras1 and R-Ras2 reduces activation of PI3K/Akt and Erk1/2-MAPK** 427 **signaling pathways**

428 Given that R-Ras1 and R-Ras2 can activate PI3K/Akt signaling (McFall et al., 2001;
 429 Rosario et al., 2001; Murphy et al., 2002; Rong et al., 2002; Delgado et al., 2009) and
 430 Erk1/2-MAPK (Graham et al., 1994; Movilla et al., 1999; Rosario et al., 1999), we
 431 examined these pathways in the optic nerve of P90 mice by Western blot using
 432 antibodies against phosphorylated Akt and Erk (active versions)(Fig. 3A). We found a
 433 reduction of both Akt phosphoepitopes T308 and S473 in single and double mutants
 434 (Fig. 3A), indicating a decrease in PI3K/Akt activity in R-Ras1- and R-Ras2-deficient
 435 adult (P90) mice. We then analyzed S6K activity, a kinase that regulates mTOR, by
 436 measuring S6 phosphorylation levels. We confirmed a significant decrease in the
 437 activity of the PI3K/Akt pathway in the absence of R-Ras1 and/or R-Ras2, with no
 438 change in the total levels of these proteins (Fig. 3A). We also examined activity of the
 439 Erk1/2-MAPK pathway in our mutant mice, observing a reduction in Erk1/2
 440 phosphorylation in the single- and double-mutant mice relative to the controls. We
 441 found that activation of the PI3K/Akt and Erk1/2-MAPK pathways was weaker in mice
 442 lacking one or both of these GTPases, which suggests that both proteins coordinate the
 443 activity of these two pathways (Fig. 3B).

444 Using immunohistochemical staining for Olig2 at different stages of OPC
 445 differentiation (E12.5, E14.5, P0, P15), we did not detect differences in
 446 oligodendrogenesis between double-mutant and control mice. The Olig2
 447 immunostaining suggested that normal oligodendrocyte migration occurs in double-

mutant mice, as OPCs born at E12.5 and E15.5 normally colonized the optic nerve and corpus callosum tracts (data not shown), as previously reported (Spassky et al., 2002; de Castro F., 2013). We also evaluated OL proliferation using BrdU labelling at different developmental stages (E14.5, E18.5, P0 and P15), finding no differences between double-mutant and control mice (data not shown). These experiments show that the absence of R-Ras1 and/or R-Ras2 does not affect OPC genesis, migration or proliferation, and rather that R-Ras1 and R-Ras2 contribute to postmitotic oligodendroglia differentiation to form mature OLs.

Next, we analyzed whether decreased activation of the PI3K/Akt and Erk1/2-MAPK pathways affected OL survival. We assessed the number of apoptotic cells in the optic nerve and corpus callosum with an antibody against active/cleaved caspase-3 in double-mutant and control mice. Quantification of caspase-3-positive cells in the optic nerve at P30 showed increased apoptosis in double-mutant relative to control mice (45.28 ± 17.39 cells/mm² in double-mutants and 11.13 ± 8 cells/mm² in control mice; $p=0.012$. Fig. 3C,D). So, dampened Erk1/2-MAPK and/or PI3K/Akt signaling may diminish cell survival, producing fewer OLs in R-Ras1- and R-Ras2-deficient mice.

Expression of typical myelin proteins is also reduced in *R-Ras1*^{-/-}, *R-Ras2*^{-/-} and *R-Ras1*^{-/-}; *R-Ras2*^{-/-} double-mutant mice

Given that OLs are the only cell type responsible for myelin production in the CNS, we wanted to determine how the reduced OL populations affected the amount of myelin sheathing the axons of mutant mice. We conducted a histological analysis using coronal sections of the adult brain (P90) and discovered a decrease in the corpus callosum in double-mutant mice compared to controls (Fig. 4A). Quantification revealed a decrease in average corpus callosum thickness in *R-Ras1*^{-/-}; *R-Ras2*^{-/-} (168 ± 11.5 μm) compared to controls (360 ± 44.5 , $p<0.0001$; Fig. 4B). Since we found no significant reduction in the

number of axons forming this tract (3705 ± 943 axons in control mice and 4377 ± 1137 axons in $R-Ras1^{-/-};R-Ras2^{-/-}$), its reduced size could reflect a deficit in the amount of myelin in these double-mutant mice. We then examined the corpus callosum and optic nerve from adult (P90) mice using immunohistological staining with specific antibodies against the myelin marker protein MBP (myelin basic protein). We saw a dramatic reduction in the amount of myelin enveloping axons in double-mutant mice compared to controls (Fig. 4 C,D).

We confirmed the decrease in myelin from adult (P90) optic nerve homogenates by Western blots using antibodies against MBP and myelin-associated glycoprotein (MAG) from adult mice lacking R-Ras1 and/or R-Ras2 and controls (Fig. 4E). Specifically, levels of MAG and MBP protein were lower in single and double mutants compared to control mice (MAG: $R-Ras1^{-/-}$ = $27.12 \pm 13.28\%$ reduction, $p=0.008$; $R-Ras2^{-/-}$ = $36.35 \pm 9.45\%$ reduction, $p=0.00263$; and the double mutant = $47.18 \pm 13.19\%$ reduction, $p=0.00345$. MBP: $R-Ras1^{-/-}$ = $30.76 \pm 18.40\%$ reduction, $p=0.0057$; $R-Ras2^{-/-}$ = $43.64 \pm 20.53\%$ reduction, $p=0.00144$; and $R-Ras1^{-/-};R-Ras2^{-/-}$ = $56.53 \pm 19.03\%$ reduction, $p=0.00016$ (Fig. 4G). In addition, expression of MAG and MBP in the corpus callosum (Fig. 4E) and spinal cord (data not shown) confirmed that the levels of myelin were reduced dramatically in the major myelinated CNS tracts in the absence of R-Ras1 and R-Ras2 (MAG $R-Ras1^{-/-};R-Ras2^{-/-}$ = $27.52 \pm 15.91\%$ reduction, $p=0.004$; MBP $R-Ras1^{-/-};R-Ras2^{-/-}$ = $55.48 \pm 20.53\%$ reduction, $p<0.0001$, Fig. 4F).

Myelin sheath thickness is reduced in $R-Ras1^{-/-}$, $R-Ras2^{-/-}$ and $R-Ras1^{-/-};R-Ras2^{-/-}$ mice

To further examine the ultrastructure of myelin tracts, we analyzed the optic nerves from $R-Ras1^{-/-}$, $R-Ras2^{-/-}$, double-mutant and control adult mice (P90) with electron microscopy (EM). We found that the myelin sheath was thinner in single and double

mutants compared to controls (Fig. 5A). Morphometric quantification of the g-ratios for individual fibers compared to the respective axon diameter in the optic nerve (presented as scatter plots) confirmed the reduction in myelin sheath thickness in *R-Ras1^{-/-}* and *R-Ras2^{-/-}* mice that was more pronounced in double-mutant compared to control mice (Fig. 5C). Specifically, we quantified significant increases in the mean value of the g-ratio of single (*R-Ras1^{-/-}*=0.87±0.04, p<0.0001, and *R-Ras2^{-/-}*=0.8±0.08, p<0.0001) and double-mutant mice (*R-Ras1^{-/-};R-Ras2^{-/-}*=0.89±0.06, p<0.0001) compared to controls (0.75±0.09).

To check whether there was a change in the axonal diameter of double mutants compared with the controls, we classified the axons according to their diameter (Fig. 5F). The double mutants showed an increase in the number of axons of lower caliber associated with a decrease in axons of greater diameter (*R-Ras1^{-/-};R-Ras2^{-/-}* = 42% increase in axons <400 nm, p<0.0001 and 29% reduction in axons >1000 nm, p=0.0002).

Regardless of axon caliber, we found a clear thinning of the myelin sheath in single (*R-Ras1^{-/-}* =105±53 nm, p<0.0001; *R-Ras2^{-/-}*=159±75 nm, p<0.0001) and double mutants (*R-Ras1^{-/-};R-Ras2^{-/-}*=73±40 nm, p=0.0001) relative to controls (251±60 nm) (Fig. 5E).

We quantified the number of axons that were myelinated, finding that in the absence of *R-Ras1* there was a decrease in the amount of myelin (Fig. 4E,G, 5A,B,C,E) without changes in the number of myelinated axons (Fig. 5D) which indicates that these axons were covered by a thinner myelin sheath. However, the absence of *R-Ras2* produced a 30% reduction in the number of myelinated axons concurrent with a loss of myelin. The most drastic phenotype was presented by the double mutant, in which there was a 75% decrease in number of myelinated axons. In addition, these mice *R-Ras1^{-/-};R-Ras2^{-/-}* show a great decrease in the amount of myelin, this indicates that these axons are coated

523 by a very thin myelin sheath, raising the value of the g-ratio. These results demonstrate
 524 the hypomyelination of the optic nerve in mice lacking R-Ras1 and/or R-Ras2. The
 525 phenotype of the double mutant corresponds to the sum of the defects observed in the
 526 single mutants.

527 We then analyzed the structure, degree and periodicity of compaction of the myelin
 528 sheaths at a higher magnification and found no differences among mutant and control
 529 mice (Fig. 5A,B). However, there were clearly fewer turns in the myelin sheaths from
 530 single mutants and even fewer in double mutants (Fig. 5B). Thus, we conclude that the
 531 reduced myelin thickness arises from fewer myelin layers. The phenotype of the double
 532 mutant indicates that R-Ras1 and R-Ras2 play additive roles in myelination.

533 **R-Ras1 and R-Ras2 are necessary for proper oligodendrocyte differentiation**

534 To evaluate whether the observed myelin loss arose from altered OPC differentiation
 535 into mature OLs, we stained brain sections from mice at the most active stages of
 536 myelination *in vivo* (P15). The antibody used was against O4 (a sulfatide and pro-
 537 oligodendroblast antigen), which is a marker for cell bodies and processes from late
 538 precursors and immature pre-myelinating OLs (Sommer and Schachner, 1981; Dawson
 539 et al., 2000; Woodruff et al., 2001; Ramos et al., 2011). We found increased intensity in
 540 O4-labeling in the corpus callosum, which suggests an alteration in the degree of OL
 541 differentiation in double mutants compared to controls (Fig. 6A,B). We then performed
 542 dual immunohistochemistry with anti-Tcf4, a specific marker of pre-myelinating
 543 immature OLs (Emery, 2010), and anti-Olig2, which recognizes the complete
 544 oligodendrocytic lineage. We found a significant increase in the population of immature
 545 OLs (Tcf4⁺) in double-mutant compared to P15 control mice (Fig. 6C). The proportion
 546 of immature OLs (Tcf4⁺) relative to the total OL population (Olig2⁺) almost doubled in
 547 *R-Ras1*^{-/-};*R-Ras2*^{-/-} mutants relative to control mice (100±7% for controls and 191±39%

548 for *R-Ras1^{-/-};R-Ras2^{-/-}*, $p=0.016$; Fig. 6C,D). We observed that the increase in Tcf4 was
 549 maintained at P30 ($100\pm 20\%$ for controls and $255\pm 14\%$ for *R-Ras1^{-/-};R-Ras2^{-/-}*,
 550 $p=0.002$; Fig. 6D) and at P120 ($100\pm 27\%$ for controls and $170\pm 53\%$ for *R-Ras1^{-/-};R-*
 551 *Ras2^{-/-}*, $p=0.017$; Fig. 6D). We found a significant increase in the population of
 552 immature OLs, not only in early postnatal stages (P15 and P30) but also in adult mice
 553 (P120). Besides, double immunohistochemical staining in adult mice (P120) with anti-
 554 Olig2 and anti-CC1, a marker of mature OLs, showed, as expected, a significant
 555 reduction in the proportion of mature OLs in the double mutant ($35.8\pm 8.6\%$ CC1/Olig2
 556 positive cells) compared with the control ($83.8\pm 0.9\%$ CC1/Olig2 positive cells,
 557 $p=0.0006$, Fig. 6 E,F). Therefore R-Ras1 and R-Ras2 seem to be necessary for the
 558 adequate maturation of OLs.
 559 To test whether the lack of R-Ras1 and R-Ras2 dampened OL maturation, we prepared
 560 enriched OL cultures from the cortex and optic nerve of newborn *R-Ras1^{-/-};R-Ras2^{-/-}*
 561 mice and their control littermates. We found that by 14 DIV, OLs from the double-
 562 mutant mice expressed CNPase and formed a more simplified network of processes
 563 than those from control mice, suggesting that OL maturation is affected by loss of R-
 564 Ras1 and R-Ras2 (Fig. 6G). After labeling with anti-CNPase and anti-Olig2 antibodies,
 565 we classified OL morphology as having either simple (primary and secondary) or
 566 complex (tertiary or myelin network) processes to reflect the changes associated with
 567 OL differentiation. This quantification of cell morphology (introduced by Kremer et al.,
 568 2009) revealed distinct differences in OL maturation between *R-Ras1^{-/-};R-Ras2^{-/-}* and
 569 control mice. OLs from R-Ras1- and R-Ras2-deficient mice had more simple processes
 570 than control mice at the expense of complex processes ($45.7\pm 12.69\%$ increase for *R-*
 571 *Ras1^{-/-};R-Ras2^{-/-}* relative to the control, $p=0.0106$; Fig. 6H). So, we conclude that OLs in
 572 double-mutant mice acquire a simpler morphology with less complex networks of

573 processes, indicating that R-Ras1 and R-Ras2 are essential for proper morphological
 574 differentiation *in vitro*.

575 **R-Ras1 and R-Ras2 modify the size of the nodes of Ranvier and axon conduction**
 576 **velocity in the optic nerve**

577 Myelin sheathes axons in segments separated by nodes of Ranvier, which are short and
 578 periodic interruptions in the myelin sheath (Fig. 7B). Given the observed
 579 hypomyelination in the optic nerve and corpus callosum of the double-mutant mice, we
 580 analyzed the gross structure of the nodal region by immunostaining against a protein
 581 located in the paranodal region, Caspr (Kamasawa et al., 2005; Murcia-Belmonte et al.,
 582 2016). Confocal microscopy of longitudinal sections of the optic nerves from adult mice
 583 (P90) immunostained with an antibody against Caspr revealed more paranodal regions
 584 in the double-mutant mice than controls (80.85 ± 19.71 paranodes/ $67 \times 67 \mu\text{m}$ for the
 585 double mutant and 54.09 ± 14.22 paranodes/ $67 \times 67 \mu\text{m}$ for the control, $p=0.000124$; Fig.
 586 7A,E). Indeed, we detected more Caspr protein in the adult (P90) double mutants
 587 relative to control mice after probing immunoblots of optic nerve homogenates for
 588 Caspr ($p=0.016$; Fig. 7C). The paranodal increase in the double mutant indicates a
 589 shorter internodal length, generating shorter myelin sheaths compared with controls
 590 (Savvaki et al., 2008) (Fig. 7D). Altered myelination may also correlate with aberrant
 591 nodal and paranodal structures (Savvaki et al., 2008; Tanaka et al., 2009; Lee et al.,
 592 2011; Murcia-Belmonte et al., 2016). After classification of the different nodes and
 593 paranodes according to their length, we did not detect differences in paranode length
 594 (Fig. 7F). In contrast, we revealed a dramatic increase in the proportion of shorter nodes
 595 (less than 0.5 microns) in *R-Ras1^{-/-};R-Ras2^{-/-}* mice relative to controls ($30 \pm 4.5\%$ for
 596 double mutant and $7.4 \pm 5.1\%$ for controls, $p=0.004$; Fig. 7A boxed insert, G).
 597 Accordingly, these double-mutant mice had fewer long nodes (between 1 and 1.5

microns: $6.95 \pm 4.05\%$ for $R-Ras1^{-/-}; R-Ras2^{-/-}$ and $25.65 \pm 6.05\%$ for control mice, $p=0.011$; Fig. 7A boxed insert, G). As the number of nodes of Ranvier and internodes increased, they became closer together (a decrease of approx. 15% in length) in the absence of R-Ras1 and R-Ras2.

The decreased myelin sheath thickness and the presence of shorter nodes could provoke abnormal conduction of nerve impulses in the major CNS myelinated tracts (Richardson et al., 2000; Bakiri et al., 2011). Thus, we measured the conduction velocity of nerve impulses along the optic nerve *in vivo*. We implanted recording electrodes into the dorsal part of the lateral geniculate nucleus of our four groups of mice (Fig. 8A-C) and stimulated the animals bilaterally with light flashes. As previously described (Wiggins et al., 1982; Meeren et al., 1998), flash stimulation evokes an early positive-negative-positive field potential followed by some late oscillatory components. The early positive component (P1, Fig. 8C) presented latencies similar for the four groups of adult mice (P120) (9.58 ± 1.09 ms for controls; 9.73 ± 1.67 ms for $R-Ras1^{-/-}$, $p=0.542$; 10.32 ± 2.38 ms for $R-Ras2^{-/-}$, $p=0.945$; and 9.77 ± 1.35 ms for $R-Ras1^{-/-}; R-Ras2^{-/-}$, $p=0.715$; Fig. 8D), which confirmed the presence of unaffected axons in the optic nerve (see above). These latencies were in the range of unitary activation of ganglion cells by photic stimulation in mice (Lintas et al., 2013). The negative component of the evoked field potential presented successive downward sags and a total long duration in mutant mice compared to controls (Fig. 8C). These successive negative waves suggest a delayed depolarization of geniculate neurons from arriving ganglion axon terminals. Indeed, a quantitative analysis of the latency of visually evoked potentials showed a significant increase in their latency in single and double mutant mice relative to control mice (19.19 ± 2.90 ms for controls; 23.08 ± 1.51 ms for $R-Ras1^{-/-}$, $p=0.00081$; 24.51 ± 2.71 ms for $R-Ras2^{-/-}$, $p=0.000385$; and 26.36 ± 2.22 ms for $R-Ras1^{-/-}; R-Ras2^{-/-}$, $p=0.0000022$; Fig. 8E). Although

623 we found alterations in conduction velocity in the two single mutant mice, we found the
624 most dramatic differences in the double mutant. These results strongly suggesting that
625 R-Ras1 and R-Ras2 have cooperative and non-redundant functions. Consequently, our
626 observed structural and electrophysiological alterations reveal that R-Ras1 and R-Ras2
627 are essential to achieve the correct velocity for nerve impulse conduction in myelinated
628 CNS tracts.
629

630 Discussion

631 Here we provide *in vivo* evidence that R-Ras1 and R-Ras2 play an essential role in
632 regulation of myelination by controlling fundamental parameters of OL survival and
633 differentiation. Our data demonstrate that mice lacking R-Ras1 and/or R-Ras2 showed
634 hypomyelination in major CNS tracts, reducing the conduction velocity of nerve
635 impulse through them.

636 Loss of either R-Ras1 or R-Ras2 reduced the number of OLs, but a more dramatic
637 reduction occurred with the loss of both. Hence, R-Ras1 and R-Ras2 may cooperatively
638 maintain the OL population. As the double mutant induced the most severe phenotype,
639 R-Ras1 and R-Ras2 do not seem functionally redundant and cannot compensate for
640 each other. We acknowledge that the classical Ras members were not modified and did
641 not compensate for the loss of R-Ras (data not shown).

642 We also detected clear differences in OL differentiation and maturation in these mutant
643 mice. Indeed, our double-mutant mice more strongly expressed markers of
644 premyelinating OLs, associated with lower expression of markers of maturity. OPCs
645 undergo stereotyped morphological changes as they differentiate (Kremer et al., 2009).
646 Specifically, oligodendroglial cells in dissociated cultures extend cell processes until
647 they acquire a truly branched morphology (Ishii et al., 2012; Zuchero et al., 2015). We
648 found that R-Ras1- and R-Ras2-deficient OLs formed a simpler network of processes
649 than control OLs, suggesting that loss of R-Ras1 and R-Ras2 alters oligodendrocyte
650 maturation *in vitro* and *in vivo*.

651 Defects in OL differentiation and maturation hinder myelination (Wolswijk, 1998;
652 Kuhlmann et al., 2008; Kremer et al., 2011). When we quantified essential myelin
653 proteins in the optic nerve and corpus callosum, we discovered distinct hypomyelination
654 in the absence of R-Ras1 and R-Ras2. Specifically, MAG and MBP expression

655 gradually decreased in these mutants, while a more significant decrease was evident in
656 the double mutants. Electron microscopy analysis of transverse optic nerve sections
657 from adult mice (P90) illustrated how axons possessed thinner myelin sheaths,
658 regardless of axon diameter. *R-Ras1*^{-/-} and *R-Ras2*^{-/-} showed different g-ratio profiles,
659 which could suggest a specific role for each of these GTPases in specific subpopulations
660 of OLs. While we found a gradual decrease in myelin sheath thickness in single
661 mutants, this decrease was more dramatic in the absence of both R-Ras1 and R-Ras2.
662 Despite the dramatic decrease in axonal myelin thickness in our mutants, we observed
663 no alterations in the degree of sheath compaction. These results suggest that the
664 mechanism responsible for assembling myelin sheaths around axons is independent of
665 R-Ras1 and R-Ras2.

666 The decrease in myelin production in the absence of R-Ras1 and R-Ras2 was much
667 more drastic than the loss of OLs. This result indicates that the surviving OLs are
668 immature and incapable of myelinating axons correctly. We discovered distinct myelin
669 deficiency in axons of all calibers, although not all fibers had hypomyelination. We
670 propose that CNS axons can differ in their proclivity to acquire a myelin sheath, as
671 suggested by (Nave and Werner, 2014). Although axon diameter was comparable
672 between mutant and control mice, we noted a tendency towards a reduced axon caliber
673 in mutants lacking R-Ras1 and/or R-Ras2, consistent with findings that OLs condition
674 axon caliber (Hildebrand and Hahn, 1978; de Waegh et al., 1992; Hildebrand et al.,
675 1993; Sanchez et al., 1996; Goebbels et al., 2010). Myelination may require
676 communication between axons, astrocytes and OLs to determine myelin sheath
677 thickness (Camargo et al., 2017). However, the contributions of each cell type to sheath
678 thickness remains unknown. The absence of R-Ras1 and R-Ras2 in neuron-free cultures
679 suggests an essential role for these GTPases in OPC differentiation. This hypothesis

680 accounts for our observed alterations in myelination. We note that the influence of R-
681 Ras1 and R-Ras2 on neurons and/or astrocytes was not explored in detail in our current
682 study.

683 Thus, downregulation of the PI3K/Akt and Erk1/2-MAPK pathways could induce
684 hypomyelination, smaller OL population, diminished cell survival and increased
685 proportion of immature OLs in the absence of R-Ras1 and R-Ras2. Increased activity of
686 the PI3K/Akt pathway, either by inhibiting PTEN or constitutively activating Akt in
687 OLs, does produce hypermyelination without altering OPC proliferation or the final
688 number of mature OLs (Flores et al., 2008; Goebbels et al., 2010). Moreover, altered
689 PI3K/Akt signaling affects OL differentiation. Specifically, inhibition of mTOR, an
690 effector of this pathway, blocks OL differentiation and preserves them in a
691 premyelinating state associated with no myelin production (Tyler et al., 2009; Gaesser,
692 2016). Likewise, overactivation of the Erk1/2-MAPK pathway in OLs provokes
693 hypermyelination in major CNS tracts (Ishii et al., 2013). Conversely, loss of Erk1/2 in
694 mature OLs decreases the amount of myelin with a concomitant reduction in the size of
695 OL population due to poor OL viability (Ishii et al., 2014). The phenotype we described
696 in R-Ras1- and R-Ras2-deficient mice could result from a combined effect of de-
697 activation of both the PI3K/Akt and Erk1/2-MAPK pathways. The relationship between
698 R-Ras1 and R-Ras2 to PI3K/Akt and Erk1/2-MAPK signaling activation must be
699 addressed in future studies. However, we do propose that R-Ras1 and R-Ras2 are
700 upstream effectors of both pathways and adequately orchestrate their signaling to
701 maintain not only survival but also correct OL differentiation.

702 Efficacy of neural transmission occurs through specific variables, such as myelin
703 thickness or node and internode length (Waxman, 1980, 1997; Zimmermann and Dours-
704 Zimmermann, 2008; Bekku et al., 2010). Hypomyelination correlates with slower

705 conduction velocities, as described in other mouse models that overexpress or lack
706 distinct myelin proteins (Robaglia-Schlupp et al., 2002; Michailov et al., 2004; Lee et
707 al., 2011). Some studies suggest weaker myelination yields slower nerve conduction
708 velocities and abnormal node or paranode structures (Tanaka et al., 2009; Lee et al.,
709 2011). A decrease in newly generated OLs may change myelin structures and induce a
710 progressive decrease in axonal conduction velocity in the corpus callosum (Schneider et
711 al., 2016). Our data demonstrate that in the absence of R-Ras1 and R-Ras2, shortening
712 of the nodes of Ranvier and internodes accompanies hypomyelination, which may cause
713 the reduced conduction velocity we observed in the optic tract. However, we cannot
714 exclude that the absence of R-Ras1 and R-Ras2 affects other factors like ion channel
715 distribution or other structural proteins in the nodal or paranodal regions. This remains
716 an area for future studies.

717 To-date, R-Ras1 and R-Ras2 activity in leukodystrophias has not been explored. The
718 accepted animal model for multiple sclerosis, experimental autoimmune
719 encephalomyelitis (EAE), is attenuated in R-Ras1^{-/-} because of an increase in
720 tolerogenic dendritic cells and natural regulatory T cells (Ray et al., 2014). After our
721 current results, we strongly suggest that the roles of R-Ras1 and R-Ras2 in
722 demyelinating diseases should be carefully studied, especially the neuropathological
723 aspects of disease.

724 In summary, we identified R-Ras1 and R-Ras2 as key elements for OL survival and
725 differentiation, acting through the synergistic activation of the PI3K/Akt and Erk1/2
726 signaling pathways. These results are separable from the classical Ras proteins, as they
727 were neither modified nor compensated for the lack of R-Ras responsiveness. Therefore,
728 we conclude that R-Ras1 and R-Ras2 GTPases are necessary for proper OL-mediated
729 myelination and regulation of correct nerve impulse transmission.

730

731 **Figure legends**

732 **Figure 1.** OLs express *R-Ras1* and *R-Ras2* in the main myelinated tracts of the CNS. **A**,
 733 Immunoblot of adult optic nerve lysates show R-Ras1, R-Ras2 and R-Ras3 expression.
 734 Two different antibodies against R-Ras1 or R-Ras2 recognized both proteins, a band of
 735 25 kDa corresponding to R-Ras1 and another of 21 kDa corresponding to R-Ras2. No
 736 bands were observed in optic nerve lysates from *R-Ras1^{-/-};R-Ras2^{-/-}* mice. R-Ras3
 737 expression was not modified in *R-Ras1^{-/-}* and/or *R-Ras2^{-/-}* showing a band of 24 kDa.
 738 (*n*=3). **B-C**, Western blot of corpus callosum (**B**) and spinal cord (**C**) extracts from
 739 control mice confirmed expression of R-Ras1, R-Ras2 and R-Ras3 in primary CNS
 740 myelinated tracts. (*n*=3). **D**, Schematic representation of the targeting strategy to
 741 generate the *R-Ras1* null mutant. A Neo cassette flanked by FRT sites was inserted into
 742 intron 1 together with two loxP sites flanking exons 2 and 6. The position of the primers
 743 designed for genotyping are shown by the arrows. **E**, PCR genotyping. A mixture of
 744 primer 1 and primer 2 detected the *R-Ras1^{+/+}* (~100 bp) allele by PCR and a mixture of
 745 primer 3 and primer 4 detected the *R-Ras1^{-/-}* target allele (~1000 bp). **F**, Generation of
 746 *R-Ras2^{-/-}* mice. Illustration of the retroviral insertion site of the *R-Ras2* gene in intron 1
 747 and the positions of the three primers used for genotyping. **G**, Analysis of the relative
 748 expression of *R-Ras1* and *R-Ras2* by RT-qPCR in control, *R-Ras1^{-/-}*, *R-Ras2^{-/-}* and *R-*
 749 *Ras1^{-/-};R-Ras2^{-/-}* adult mice normalizing all data to control mice. Values expressed as
 750 the mean fold-change of 3 different animals, *p*<0.0001. **H**, Longitudinal optic nerve
 751 sections from control, *R-Ras1^{-/-}*, *R-Ras2^{-/-}* and *R-Ras1^{-/-};R-Ras2^{-/-}* adult mice showing
 752 co-localization between R-Ras1 (top) and R-Ras2 (bottom, green) with Nkx2.2, an
 753 oligodendroglial cell marker (red). No staining for R-Ras1 or R-Ras2 was observed in
 754 the double-mutant mice. (*n*=3). All samples were obtained from adult mice (P90). Scale
 755 bar: 25µm.

Figure 2. OL population is significantly diminished in *R-Ras1*^{-/-}, *R-Ras2*^{-/-} and *R-Ras1*^{-/-};*R-Ras2*^{-/-} mice. **A**, Immunolabeling with anti-Olig2 (green) of longitudinal optic nerve sections from control, *R-Ras1*^{-/-}, *R-Ras2*^{-/-} and *R-Ras1*^{-/-};*R-Ras2*^{-/-} adult mice (P90), show a reduction in the OL population in the mutant mice compared with the controls. **B**, Simplified scheme of the visual tract shows the region of analysis. **C**, Quantification of the density of Olig2-positive cells per mm² shows a 19.1±7.5% decrease in *R-Ras1*^{-/-} (p=0.02), a 33.5±2.1% reduction in *R-Ras2*^{-/-} (p<0.0001) and a 42.8±11.8% reduction (p=0.003) in *R-Ras1*^{-/-};*R-Ras2*^{-/-} mice relative to controls. Reduction of OLs in the *R-Ras1*^{-/-} mutant mice was significantly less than that observed in the *R-Ras2*^{-/-} (p=0.003) and *R-Ras1*^{-/-};*R-Ras2*^{-/-} (p=0.02) mutant mice. The bar graph represents the mean and SD for the number of Olig2-positive cells per mm² from six different experiments (n=6). Scale Bars: 75 μm.

Figure 3. R-Ras1 and R-Ras2 are necessary for OL survival driven by PI3K/Akt and Erk1/2-MAPK signaling. **A**, Western blot analysis of phospho-Akt (T308), phospho-Akt (S473) and phospho-S6 in optic nerve lysates of adult mice (P90) shows the PI3K/Akt pathway was altered in the absence of R-Ras1 and/or R-Ras2. Phosphorylated proteins were significantly reduced in mutant mice compared to controls. (Bottom) Western blot analysis shows decreased phosphorylated Erk1/2 (T202/Y204) in adult optic nerve lysates from *R-Ras1*^{-/-}, *R-Ras2*^{-/-} and *R-Ras1*^{-/-};*R-Ras2*^{-/-} mice compared to controls. Graphs show densitometric analysis of phosphorylated Akt, S6 and Erk1/2 normalized to total protein levels compared to controls (100%, n=4): P-Akt (T308) *R-Ras1*^{-/-} 78.5±6.51% reduction (p<0.0001), *R-Ras2*^{-/-} 35.3±12.80% reduction (p=0.0035), *R-Ras1*^{-/-};*R-Ras2*^{-/-} 34.5±15.23% reduction (p=0.007); P-Akt (S473) *R-Ras1*^{-/-} 49.2±1.20% reduction (p<0.0001), *R-Ras2*^{-/-} 53.2±15.92% reduction (p=0.0044), *R-Ras1*^{-/-};*R-Ras2*^{-/-} 62.9±4.92% reduction (p=0.0001); p-S6 *R-Ras1*^{-/-} 62.6±6.8% reduction

781 ($p<0.0001$), *R-Ras2*^{-/-} 50.9±15.2% reduction ($p=0.0002$), *R-Ras1*^{-/-};*R-Ras2*^{-/-}
 782 65.2±23.5% reduction ($p=0.0005$); p-Erk1/2 *R-Ras1*^{-/-} 45.4±25.8% reduction ($p=0.004$),
 783 *R-Ras2*^{-/-} 55.6±15.3% reduction ($p<0.0001$), *R-Ras1*^{-/-};*R-Ras2*^{-/-} 68.5±20.3% reduction
 784 ($p<0.0001$). **B**, Schematic representation of the pathways downstream of R-Ras1 and R-
 785 Ras2. Discontinuous lines imply indirect activation or inhibition. **C**, Bar graph shows
 786 the mean number of caspase-3-positive cells per mm² observed in P30 optic nerves from
 787 *R-Ras1*^{-/-};*R-Ras2*^{-/-} (45.28±17.39) compared with controls (11.14±8.01, $p=0.0124$; $n=3$).
 788 **D**, Immunostaining of longitudinal sections of optic nerves at P30 with anti-cleaved-
 789 caspase-3 reveals increased cell apoptosis in the *R-Ras1*^{-/-};*R-Ras2*^{-/-} mice compared to
 790 controls ($n=3$). Scale Bar=25 μ m.

791 **Figure 4.** Myelin decrease in the absence of R-Ras1 and/or R-Ras2. **A**, Coronal sections
 792 from adult (P90) mouse brains stained with DAPI show a remarkable reduction in the
 793 thickness of the corpus callosum in the double mutant compared with the control.
 794 Lower-magnification images of the corpus callosum shown in the boxed insert
 795 (interaural 4.40-4.76 mm and bregma 0.61-0.97 mm; (Paxinos and Franklin, 2013). **B**,
 796 Quantification of corpus callosum thickness in these coronal sections shows a decrease
 797 in *R-Ras1*^{-/-};*R-Ras2*^{-/-} compared with control. Corpus callosum thickness was analyzed
 798 in several positions: position 0 in x-axis means a measurement in middle line (*R-Ras1*^{-/-}
 799 ;*R-Ras2*^{-/-} 169.7±16.5 μ m, control 428.6±43.1 μ m, $p<0.0001$); position 0.5 is a
 800 measurement in cingulate cortex (*R-Ras1*^{-/-};*R-Ras2*^{-/-} 158.7±7.8 μ m, control 321.3±40.7
 801 μ m, $p=0.0002$ in right, *R-Ras1*^{-/-};*R-Ras2*^{-/-} 155.1±15.8 μ m, control 342.4±30.2 μ m,
 802 $p<0.0001$ in left); position 1 is a measurement in secondary motor cortex (*R-Ras1*^{-/-};*R-*
 803 *Ras2*^{-/-} 184.3±18.2 μ m, control 365.9±59.5 μ m, $p=0.0011$ in right, *R-Ras1*^{-/-};*R-Ras2*^{-/-}
 804 181.8±29.9 μ m, control 408.2±41.6 μ m, $p<0.0001$ in left); position 1.5 is a
 805 measurement in primary motor cortex (*R-Ras1*^{-/-};*R-Ras2*^{-/-} 158.9±12.3 μ m, control

305.9±66.8 μm, $p=0.005$ in right, $R-RasI^{-/-};R-Ras2^{-/-}$ 166.7±31.2 μm, control
 352.5±30.3 μm, $p<0.0001$ in left). **C-D** Dual staining of longitudinal sections of adult
 (P90) corpus callosum (**C**) and optic nerves (**D**) with anti-MBP and anti-NF200 (red)
 reveals myelin deficits in $R-RasI^{-/-};R-Ras2^{-/-}$ mice relative to controls. **E**, Immunoblot
 of corpus callosum lysates from P90 double-mutant mice compared with controls also
 shows this reduction in MAG and MBP. Western blot of adult (P90) optic nerve lysates
 confirmed a significant decrease in the myelin marker protein expression, like MAG
 and MBP in single and double mutants compared to controls. (n=3). **F**, Significant
 decrease in MAG and MBP expression in the corpus callosum. Bar graph represents
 mean ± SD of the change relative to the control of measurements normalized to
 GAPDH from three different experiments: MAG $R-RasI^{-/-};R-Ras2^{-/-}$ 72.48±15.91%
 ($p=0.004$); MBP $R-RasI^{-/-};R-Ras2^{-/-}$ 44.52±20.53% ($p<0.0001$). **G**, Significant
 decrease in MAG and MBP expression in the optic nerve. Bar graph represents mean ±
 SD of the change relative to the control of measurements normalized to GAPDH from
 three different experiments: MAG $R-RasI^{-/-}$ 72.89±13.29% ($p=0.0083$), $R-Ras2^{-/-}$
 63.65±9.45% ($p=0.0026$), $R-RasI^{-/-};R-Ras2^{-/-}$ 52.82±13.19% ($p=0.0035$); MBP $R-RasI^{-/-}$
 69.24±18.41% ($p=0.0057$), $R-Ras2^{-/-}$ 56.36±20.54% ($p=0.0014$), $R-RasI^{-/-};R-Ras2^{-/-}$
 43.47±19.03% ($p=0.00016$). n=3. Scale Bar= 500 μm in A; 5 μm in C and D.

Figure 5. Thinner myelin sheath in $R-RasI^{-/-}$, $R-Ras2^{-/-}$ and $R-RasI^{-/-};R-Ras2^{-/-}$ adult
 (P90) mutant mice. **A**, Transverse sections of the optic nerve from adult (P90) control,
 $R-RasI^{-/-}$, $R-Ras2^{-/-}$ and $R-RasI^{-/-};R-Ras2^{-/-}$ mice analyzed by electron microscopy show
 a significant decrease of myelin in single and double mutants compared with controls.
B, Higher magnification images show no differences in myelin structure, compaction
 and periodicity in mutant mice compared to controls. However, $R-RasI^{-/-}$, $R-Ras2^{-/-}$ and
 more dramatically $R-RasI^{-/-};R-Ras2^{-/-}$, show less wrapping of myelinated axons

831 compared to controls. **C**, Scatter plots show the morphometric quantification of g-ratios
 832 (y-axis) of individual fibers relative to the respective axon diameters (x-axis) from optic
 833 nerves. Significant increase in g-ratios were found in *R-Ras1*^{-/-} (0.87 ± 0.04 , $p=0.000012$,
 834 $n=924$ axons analyzed), *R-Ras2*^{-/-} (0.8 ± 0.08 , $p=0.000011$, $n=1014$ axons analyzed) and
 835 *R-Ras1*^{-/-};*R-Ras2*^{-/-} (0.89 ± 0.06 , $p=0.000072$, $n=1037$ axons analyzed) compared to
 836 controls (0.75 ± 0.09 , $n=764$ axons analyzed). **D**, Graph shows the percentage of
 837 myelinated axons present in the optic nerve of *R-Ras1*^{-/-} = $102 \pm 2.7\%$, *R-Ras2*^{-/-} =
 838 $72.1 \pm 5.2\%$ and *R-Ras1*^{-/-};*R-Ras2*^{-/-} = $23.9 \pm 2.5\%$ compared to the control = $100 \pm 2.8\%$.
 839 Significant differences were observed in the *R-Ras2*^{-/-} ($p<0.0001$) and the double-mutant
 840 mice ($p<0.0001$). **E**, Scatter plots show the variation of myelin thickness with respect to
 841 the diameter of axons in single and double mutants compared to the control (control =
 842 251 ± 60 nm, $n=764$ axons analyzed; *R-Ras1*^{-/-} = 105 ± 53 nm, $p<0.0001$, $n=924$ axons
 843 analyzed; *R-Ras2*^{-/-} = 159 ± 75 nm, $p<0.0001$, $n=1014$ axons analyzed; *R-Ras1*^{-/-};*R-Ras2*^{-/-}
 844 = 73 ± 40 nm, $p<0.0001$, $n=1037$ axons analyzed). **F**, Graph shows the percentage of
 845 axons classified according to their diameters in control and double-mutant mice.
 846 Compared to the control, *R-Ras1*^{-/-};*R-Ras2*^{-/-} mice showed a significant increase in the
 847 smallest axons, measuring less than 600 nm, (control = 30% , *R-Ras1*^{-/-};*R-Ras2*^{-/-} =
 848 42.6% of axons, $p<0.0001$) and a significant decrease in axons measuring more than
 849 1000 nm (control = 30.3% , *R-Ras1*^{-/-};*R-Ras2*^{-/-} = 21.5% of axons, $p=0.0002$). All
 850 samples were obtained from adult mice (P90). $n=3$. Scale Bars= 500 nm in A; 250 nm
 851 in B.

852 **Figure 6.** R-Ras1 and R-Ras2 play a crucial role in OL differentiation. **A**, Mirror
 853 images of coronal brain sections from P15 control and *R-Ras1*^{-/-};*R-Ras2*^{-/-} mice
 854 immunolabeled with an anti-O4 antibody (red). Pictures correspond to the corpus
 855 callosum (interaural 2.36-2.48 mm and bregma -1.43 mm (Paxinos and Franklin, 2013).

856 More intense staining occurred in *R-Ras1^{-/-};R-Ras2^{-/-}* mice, indicating an increase in the
 857 proportion of pre-myelinating OLs in double mutants relative to controls. **B**, Schematic
 858 representation of different O4 immunostaining observed in double mutants compared to
 859 controls. Right hemisphere represents *R-Ras1^{-/-};R-Ras2^{-/-}* mice where the corpus
 860 callosum shows more premyelinating OLs (red) than controls (left hemisphere). **C**, Dual
 861 immunostaining with anti-Tcf4 (red) and anti-Olig2 (green) in the corpus callosum of
 862 P15 control (top) and *R-Ras1^{-/-};R-Ras2^{-/-}* (bottom) mice. Double-mutant mice showed
 863 more premyelinating OLs than controls (Tcf4/Olig2 positive cells) in P15 mice. **D**,
 864 Percentage of premyelinating OLs (Tcf4-positive cells) relative to the amount of OLs
 865 (Olig2-positive cells). Double-mutant mice show a significant increase in the number of
 866 immature OLs compared to controls. Bar graph represents a significant increase in the
 867 percentage of Tcf4-positive cells in double mutants compared with controls. (P15: *R-*
 868 *Ras1^{-/-};R-Ras2^{-/-}*=91% increase $p=0.016$; P30: *R-Ras1^{-/-};R-Ras2^{-/-}*=155% increase,
 869 $p=0.002$ and P120: *R-Ras1^{-/-};R-Ras2^{-/-}*=70% increase, $p=0.017$) ($n=3$). **E**, Double
 870 immunostaining with anti-CC1 (red) and anti-Olig2 (green) in the corpus callosum of
 871 P120 control (top) and *R-Ras1^{-/-};R-Ras2^{-/-}* (bottom) mice. Double-mutant mice showed
 872 a drastic reduction in the proportion of mature OLs compared with the controls
 873 (CC1/Olig2 positive cells). **F**, Quantification of the percentage of mature OLs
 874 (CC1positive cells) relative to the total amount of OLs (Olig2 positive cells). A
 875 significant decrease in the percentage of CC1 positive cells was found in double
 876 mutants compared with controls (*R-Ras1^{-/-};R-Ras2^{-/-}*=57.3% decrease $p=0.0006$ ($n=3$).
 877 **G**, Representative confocal images of morphologies found in primary cultures stained
 878 for CNPase (green) and Olig2 (red). After 14 DIV, OLs from double mutants show
 879 simpler morphology than controls. **H**, Schematic representation of enriched primary OL
 880 cultures from the cortex of control and *R-Ras1^{-/-};R-Ras2^{-/-}* mice shows a simpler

881 morphology in double mutants. Proportion of OLs (CNPase and Olig2 positive cells)
 882 with simple and complex processes are shown for each genotype in the bar graph. Most
 883 double-mutant OLs had simple processes ($72.85 \pm 12.7\%$, $n=101$ OLs quantified) that
 884 differed significantly from controls ($27.15 \pm 12.7\%$, $p=0.0106$, $n=121$ OLs quantified).
 885 A few double-mutant OLs had complex processes ($24.9 \pm 13.3\%$) that differed
 886 significantly from controls ($75.1 \pm 13.3\%$, $p=0.0106$). Scale Bars: $250 \mu\text{m}$ in A; $25 \mu\text{m}$ in
 887 C and E.

888 **Figure 7.** More nodes of Ranvier with shorter length generate more internodes in the
 889 absence of R-Ras1 and R-Ras2 in adult mice (P90). **A**, Double-staining of longitudinal
 890 sections of adult (P90) optic nerves with anti-Caspr (green) and anti-NF200 (red) reveal
 891 an increase in the number of paranodes (green) in the *R-Ras1^{-/-};R-Ras2^{-/-}* mice compared
 892 to controls. The distance between paranodes (nodal length) in higher magnification
 893 images (boxed insert) was shorter in double mutants than in controls. **B**, Simplified
 894 scheme representing the node of Ranvier between two internodes. **C**, Western blot of
 895 P90 optic nerve lysates shows a significant increase in Caspr protein expression in
 896 double mutants compared to controls. Bar graph shows the mean \pm SD change in
 897 densitometric measurements normalized to GAPDH and relative to controls ($p=0.016$;
 898 $n=5$). **D**, Schematic representation of the shorter nodal length and more internodes
 899 observed in the *R-Ras1^{-/-};R-Ras2^{-/-}* mice compared to control. **E**, Bar graph shows a
 900 significant increase in paranodes found in double mutants (80.85 ± 19.71
 901 paranodes/ $67 \times 67 \mu\text{m}$) compared to controls (54.09 ± 14.22 paranodes/ $67 \times 67 \mu\text{m}$) ($p=$
 902 0.000124 ; $n=4$). **F**, Paranodal length classification does not reveal any differences in *R-*
 903 *Ras1^{-/-};R-Ras2^{-/-}* compared with controls. **G**, Node classification by their length reveals
 904 more short nodes in *R-Ras1^{-/-};R-Ras2^{-/-}* mice ($30.5 \pm 4.5\%$ of nodes $<0.5 \mu\text{m}$ long) than
 905 in controls ($7.5 \pm 5.1\%$ of nodes $<0.5 \mu\text{m}$ long, $p=0.004$) at the expense of longer nodes.

906 **Figure 8.** Axonal conduction velocity was affected by the absence of *R-Ras1* and/or *R-*
907 *Ras2*. **A**, Experimental design. Alert-behaving mice received a photic stimulator (flash)
908 through a stroboscope located 30 cm in from of them. **B**, Recording electrodes
909 implanted in the left dorsal lateral geniculate nucleus. Photomicrograph illustrates
910 recording electrode location. **C**, Examples of field potentials evoked by light flash
911 stimulation at the dorsal lateral geniculate nucleus. Recordings averaged 20 times and
912 collected from representative control, *R-Ras1*^{-/-}, *R-Ras2*^{-/-}, and *R-Ras1*^{-/-};*R-Ras2*^{-/-} mice.
913 Light flash presentation indicated by an arrow. Latency to P1 and to the latest N
914 component of the evoked field potential indicated. **D**, **E**, Although no significant
915 differences were observed for latency values from flash presentation to P1, latency
916 values to the last N component of the evoked field potential were significantly larger for
917 the three experimental groups (*R-Ras1*^{-/-}, *R-Ras2*^{-/-}, and *R-Ras1*^{-/-};*R-Ras2*^{-/-}) compared
918 with controls. ***, p<0.001. All mice analyzed were adults (P120).
919

920 References

- 921 Arimura N, Kaibuchi K (2007) Neuronal polarity: from extracellular signals to
922 intracellular mechanisms. *Nat Rev Neurosci* 8:194-205.
- 923 Bakiri Y, Karadottir R, Cossell L, Attwell D (2011) Morphological and electrical
924 properties of oligodendrocytes in the white matter of the corpus callosum and
925 cerebellum. *J Physiol* 589:559-573.
- 926 Bauer NG, Richter-Landsberg C, Ffrench-Constant C (2009) Role of the
927 oligodendroglial cytoskeleton in differentiation and myelination. *Glia* 57:1691-
928 1705.
- 929 Bekku Y, Vargova L, Goto Y, Vorisek I, Dmytrenko L, Narasaki M, Ohtsuka A, Fassler
930 R, Ninomiya Y, Sykova E, Ohashi T (2010) Bral1: its role in diffusion barrier
931 formation and conduction velocity in the CNS. *J Neurosci* 30:3113-3123.
- 932 Boespflug-Tanguy O, Labauge P, Fogli A, Vaur-Barriere C (2008) Genes involved in
933 leukodystrophies: a glance at glial functions. *Curr Neurol Neurosci Rep* 8:217-
934 229.
- 935 Camargo N, Goudriaan A, van Deijk AF, Otte WM, Brouwers JF, Lodder H, Gutmann
936 DH, Nave KA, Dijkhuizen RM, Mansvelder HD, Chrast R, Smit AB, Verheijen
937 MHG (2017) Oligodendroglial myelination requires astrocyte-derived lipids.
938 *PLoS Biol* 15:e1002605.
- 939 Chan AM, Miki T, Meyers KA, Aaronson SA (1994) A human oncogene of the RAS
940 superfamily unmasked by expression cDNA cloning. *Proc Natl Acad Sci U S A*
941 91:7558-7562.
- 942 Colicelli J (2004) Human RAS superfamily proteins and related GTPases. *Sci STKE*
943 2004:RE13.
- 944 Cubelos B, Sebastian-Serrano A, Kim S, Moreno-Ortiz C, Redondo JM, Walsh CA,
945 Nieto M (2008) Cux-2 controls the proliferation of neuronal intermediate
946 precursors of the cortical subventricular zone. *Cereb Cortex* 18:1758-1770.
- 947 Dawson MR, Levine JM, Reynolds R (2000) NG2-expressing cells in the central
948 nervous system: are they oligodendroglial progenitors? *J Neurosci Res* 61:471-
949 479.
- 950 de Castro F. ZB (2013) "Migration of myelin-forming cells in the CNS," in
951 *Comprehensive Developmental Neuroscience: Cellular Migration and*
952 *Formation of Neuronal Connections*. 2:1080.
- 953 de Waegh SM, Lee VM, Brady ST (1992) Local modulation of neurofilament
954 phosphorylation, axonal caliber, and slow axonal transport by myelinating
955 Schwann cells. *Cell* 68:451-463.
- 956 Delgado P, Cubelos B, Calleja E, Martinez-Martin N, Cipres A, Merida I, Bellas C,
957 Bustelo XR, Alarcon B (2009) Essential function for the GTPase TC21 in
958 homeostatic antigen receptor signaling. *Nat Immunol* 10:880-888.
- 959 Drivas GT, Shih A, Coutavas E, Rush MG, D'Eustachio P (1990) Characterization of
960 four novel ras-like genes expressed in a human teratocarcinoma cell line. *Mol*
961 *Cell Biol* 10:1793-1798.
- 962 Emery B (2010) Regulation of oligodendrocyte differentiation and myelination. *Science*
963 330:779-782.
- 964 Flores AI, Narayanan SP, Morse EN, Shick HE, Yin X, Kidd G, Avila RL, Kirschner
965 DA, Macklin WB (2008) Constitutively active Akt induces enhanced
966 myelination in the CNS. *J Neurosci* 28:7174-7183.
- 967 Furusho M, Ishii A, Bansal R (2017) Signaling by FGF Receptor 2, Not FGF Receptor
968 1, Regulates Myelin Thickness through Activation of ERK1/2-MAPK, Which

- Promotes mTORC1 Activity in an Akt-Independent Manner. *J Neurosci* 37:2931-2946.
- Fyffe-Maricich SL, Karlo JC, Landreth GE, Miller RH (2011) The ERK2 mitogen-activated protein kinase regulates the timing of oligodendrocyte differentiation. *J Neurosci* 31:843-850.
- Gaesser JM, Fyffe-Maricich SL (2016) Intracellular Signaling Pathway Regulation of Myelination and Remyelination in the CNS. *Exp Neurol* 283:501-511.
- Gaesser JM, Fyffe-Maricich, S.L. (2016) Intracellular Signaling Pathway Regulation of Myelination and Remyelination in the CNS. *Exp Neurol* 283:501-511.
- Goebbels S, Oltrogge JH, Kemper R, Heilmann I, Bormuth I, Wolfer S, Wichert SP, Mobius W, Liu X, Lappe-Siefke C, Rossner MJ, Groszer M, Suter U, Frahm J, Boretius S, Nave KA (2010) Elevated phosphatidylinositol 3,4,5-trisphosphate in glia triggers cell-autonomous membrane wrapping and myelination. *J Neurosci* 30:8953-8964.
- Graham SM, Cox AD, Drivas G, Rush MG, D'Eustachio P, Der CJ (1994) Aberrant function of the Ras-related protein TC21/R-Ras2 triggers malignant transformation. *Mol Cell Biol* 14:4108-4115.
- Graham SM, Oldham SM, Martin CB, Drugan JK, Zohn IE, Campbell S, Der CJ (1999) TC21 and Ras share indistinguishable transforming and differentiating activities. *Oncogene* 18:2107-2116.
- Gutierrez-Erlandsson S, Herrero-Vidal P, Fernandez-Alfara M, Hernandez-Garcia S, Gonzalo-Flores S, Mudarra-Rubio A, Fresno M, Cubelos B (2013) R-RAS2 overexpression in tumors of the human central nervous system. *Mol Cancer* 12:127.
- Harrington EP, Zhao C, Fancy SP, Kaing S, Franklin RJ, Rowitch DH (2010) Oligodendrocyte PTEN is required for myelin and axonal integrity, not remyelination. *Ann Neurol* 68:703-716.
- Hildebrand C, Hahn R (1978) Relation between myelin sheath thickness and axon size in spinal cord white matter of some vertebrate species. *J Neurol Sci* 38:421-434.
- Hildebrand C, Remahl S, Persson H, Bjartmar C (1993) Myelinated nerve fibres in the CNS. *Prog Neurobiol* 40:319-384.
- Ishii A, Furusho M, Bansal R (2013) Sustained activation of ERK1/2 MAPK in oligodendrocytes and schwann cells enhances myelin growth and stimulates oligodendrocyte progenitor expansion. *J Neurosci* 33:175-186.
- Ishii A, Furusho M, Dupree JL, Bansal R (2014) Role of ERK1/2 MAPK signaling in the maintenance of myelin and axonal integrity in the adult CNS. *J Neurosci* 34:16031-16045.
- Ishii A, Fyffe-Maricich SL, Furusho M, Miller RH, Bansal R (2012) ERK1/ERK2 MAPK signaling is required to increase myelin thickness independent of oligodendrocyte differentiation and initiation of myelination. *J Neurosci* 32:8855-8864.
- Iwasawa N, Negishi M, Oinuma I (2012) R-Ras controls axon branching through afadin in cortical neurons. *Mol Biol Cell* 23:2793-2804.
- Jeffries MA, Urbanek K, Torres L, Wendell SG, Rubio ME, Fyffe-Maricich SL (2016) ERK1/2 Activation in Preexisting Oligodendrocytes of Adult Mice Drives New Myelin Synthesis and Enhanced CNS Function. *J Neurosci* 36:9186-9200.
- Kamasawa N, Sik A, Morita M, Yasumura T, Davidson KG, Nagy JI, Rash JE (2005) Connexin-47 and connexin-32 in gap junctions of oligodendrocyte somata, myelin sheaths, paranodal loops and Schmidt-Lanterman incisures: implications for ionic homeostasis and potassium siphoning. *Neuroscience* 136:65-86.

- 1019 Karnoub AE, Weinberg RA (2008) Ras oncogenes: split personalities. *Nat Rev Mol*
 1020 *Cell Biol* 9:517-531.
- 1021 Kimmelman AC, Nunez Rodriguez N, Chan AM (2002) R-Ras3/M-Ras induces
 1022 neuronal differentiation of PC12 cells through cell-type-specific activation of the
 1023 mitogen-activated protein kinase cascade. *Mol Cell Biol* 22:5946-5961.
- 1024 Komatsu M, Ruoslahti E (2005) R-Ras is a global regulator of vascular regeneration
 1025 that suppresses intimal hyperplasia and tumor angiogenesis. *Nat Med* 11:1346-
 1026 1350.
- 1027 Kremer D, Aktas O, Hartung HP, Kury P (2011) The complex world of
 1028 oligodendroglial differentiation inhibitors. *Ann Neurol* 69:602-618.
- 1029 Kremer D, Heinen A, Jadasz J, Gottle P, Zimmermann K, Zickler P, Jander S, Hartung
 1030 HP, Kury P (2009) p57kip2 is dynamically regulated in experimental
 1031 autoimmune encephalomyelitis and interferes with oligodendroglial maturation.
 1032 *Proc Natl Acad Sci U S A* 106:9087-9092.
- 1033 Kuhlmann T, Miron V, Cui Q, Wegner C, Antel J, Bruck W (2008) Differentiation
 1034 block of oligodendroglial progenitor cells as a cause for remyelination failure in
 1035 chronic multiple sclerosis. *Brain* 131:1749-1758.
- 1036 Larive RM, Abad A, Cardaba CM, Hernandez T, Canamero M, de Alava E, Santos E,
 1037 Alarcon B, Bustelo XR (2012) The Ras-like protein R-Ras2/TC21 is important
 1038 for proper mammary gland development. *Mol Biol Cell* 23:2373-2387.
- 1039 Lee X, Hu Y, Zhang Y, Yang Z, Shao Z, Qiu M, Pepinsky B, Miller RH, Mi S (2011)
 1040 Oligodendrocyte differentiation and myelination defects in OMgp null mice.
 1041 *Mol Cell Neurosci* 46:752-761.
- 1042 Lintas A, Schwaller B, Villa AE (2013) Visual thalamocortical circuits in parvalbumin-
 1043 deficient mice. *Brain Res* 1536:107-118.
- 1044 McCarthy KD, de Vellis J (1980) Preparation of separate astroglial and oligodendroglial
 1045 cell cultures from rat cerebral tissue. *J Cell Biol* 85:890-902.
- 1046 McFall A, Ulku A, Lambert QT, Kusa A, Rogers-Graham K, Der CJ (2001) Oncogenic
 1047 Ras blocks anoikis by activation of a novel effector pathway independent of
 1048 phosphatidylinositol 3-kinase. *Mol Cell Biol* 21:5488-5499.
- 1049 Medina-Rodriguez EM, Arenzana FJ, Pastor J, Redondo M, Palomo V, Garcia de Sola
 1050 R, Gil C, Martinez A, Bribian A, de Castro F (2013) Inhibition of endogenous
 1051 phosphodiesterase 7 promotes oligodendrocyte precursor differentiation and
 1052 survival. *Cell Mol Life Sci* 70:3449-3462.
- 1053 Meeren HK, Van Lujtelaar EL, Coenen AM (1998) Cortical and thalamic visual
 1054 evoked potentials during sleep-wake states and spike-wave discharges in the rat.
 1055 *Electroencephalogr Clin Neurophysiol* 108:306-319.
- 1056 Michailov GV, Sereda MW, Brinkmann BG, Fischer TM, Haug B, Birchmeier C, Role
 1057 L, Lai C, Schwab MH, Nave KA (2004) Axonal neuregulin-1 regulates myelin
 1058 sheath thickness. *Science* 304:700-703.
- 1059 Molina-Holgado E, Vela JM, Arevalo-Martin A, Almazan G, Molina-Holgado F,
 1060 Borrell J, Guaza C (2002) Cannabinoids promote oligodendrocyte progenitor
 1061 survival: involvement of cannabinoid receptors and phosphatidylinositol-3
 1062 kinase/Akt signaling. *J Neurosci* 22:9742-9753.
- 1063 Movilla N, Crespo P, Bustelo XR (1999) Signal transduction elements of TC21, an
 1064 oncogenic member of the R-Ras subfamily of GTP-binding proteins. *Oncogene*
 1065 18:5860-5869.
- 1066 Murcia-Belmonte V, Medina-Rodriguez EM, Bribian A, de Castro F, Esteban PF (2014)
 1067 ERK1/2 signaling is essential for the chemoattraction exerted by human FGF2

- and human anosmin-1 on newborn rat and mouse OPCs via FGFR1. *Glia* 62:374-386.
- Murcia-Belmonte V, Esteban PF, Martinez-Hernandez J, Gruart A, Lujan R, Delgado-Garcia JM, de Castro F (2016) Anosmin-1 over-expression regulates oligodendrocyte precursor cell proliferation, migration and myelin sheath thickness. *Brain Struct Funct* 221:1365-1385.
- Murphy GA, Graham SM, Morita S, Reks SE, Rogers-Graham K, Vojtek A, Kelley GG, Der CJ (2002) Involvement of phosphatidylinositol 3-kinase, but not RalGDS, in TC21/R-Ras2-mediated transformation. *J Biol Chem* 277:9966-9975.
- Nave KA, Werner HB (2014) Myelination of the nervous system: mechanisms and functions. *Annu Rev Cell Dev Biol* 30:503-533.
- Ness JK, Mitchell NE, Wood TL (2002) IGF-I and NT-3 signaling pathways in developing oligodendrocytes: differential regulation and activation of receptors and the downstream effector Akt. *Dev Neurosci* 24:437-445.
- Ohba Y, Mochizuki N, Yamashita S, Chan AM, Schrader JW, Hattori S, Nagashima K, Matsuda M (2000) Regulatory proteins of R-Ras, TC21/R-Ras2, and M-Ras/R-Ras3. *J Biol Chem* 275:20020-20026.
- Olsen IM, Ffrench-Constant C (2005) Dynamic regulation of integrin activation by intracellular and extracellular signals controls oligodendrocyte morphology. *BMC Biol* 3:25.
- Ono K, Hirahara Y, Gotoh H, Nomura T, Takebayashi H, Yamada H, Ikenaka K (2017) Origin of Oligodendrocytes in the Vertebrate Optic Nerve: A Review. *Neurochem Res*.
- Paxinos G, Franklin KBJ (2013) Paxinos and Franklin's the Mouse Brain in Stereotaxic Coordinates, Fourth Edition Edition: Elsevier. Academic Press.
- Pylayeva-Gupta Y, Grabocka E, Bar-Sagi D (2011) RAS oncogenes: weaving a tumorigenic web. *Nat Rev Cancer* 11:761-774.
- Qi Y, Cai J, Wu Y, Wu R, Lee J, Fu H, Rao M, Sussel L, Rubenstein J, Qiu M (2001) Control of oligodendrocyte differentiation by the Nkx2.2 homeodomain transcription factor. *Development* 128:2723-2733.
- Ramos M, Pardo B, Llorente-Folch I, Saheki T, Del Arco A, Satrustegui J (2011) Deficiency of the mitochondrial transporter of aspartate/glutamate aralar/AGC1 causes hypomyelination and neuronal defects unrelated to myelin deficits in mouse brain. *J Neurosci Res* 89:2008-2017.
- Ray A, Basu S, Miller NM, Chan AM, Dittel BN (2014) An increase in tolerogenic dendritic cell and natural regulatory T cell numbers during experimental autoimmune encephalomyelitis in Rras-/- mice results in attenuated disease. *J Immunol* 192:5109-5117.
- Richardson AG, McIntyre CC, Grill WM (2000) Modelling the effects of electric fields on nerve fibres: influence of the myelin sheath. *Med Biol Eng Comput* 38:438-446.
- Robaglia-Schlupp A, Pizant J, Norreel JC, Passage E, Saberan-Djoneidi D, Ansaldi JL, Vinay L, Figarella-Branger D, Levy N, Clarac F, Cau P, Pellissier JF, Fontes M (2002) PMP22 overexpression causes dysmyelination in mice. *Brain* 125:2213-2221.
- Romanelli RJ, Mahajan KR, Fulmer CG, Wood TL (2009) Insulin-like growth factor-I-stimulated Akt phosphorylation and oligodendrocyte progenitor cell survival require cholesterol-enriched membranes. *J Neurosci Res* 87:3369-3377.

- 1117 Rong R, He Q, Liu Y, Sheikh MS, Huang Y (2002) TC21 mediates transformation and
 1118 cell survival via activation of phosphatidylinositol 3-kinase/Akt and NF-kappaB
 1119 signaling pathway. *Oncogene* 21:1062-1070.
- 1120 Rosario M, Paterson HF, Marshall CJ (1999) Activation of the Raf/MAP kinase cascade
 1121 by the Ras-related protein TC21 is required for the TC21-mediated
 1122 transformation of NIH 3T3 cells. *EMBO J* 18:1270-1279.
- 1123 Rosario M, Paterson HF, Marshall CJ (2001) Activation of the Ral and
 1124 phosphatidylinositol 3' kinase signaling pathways by the ras-related protein
 1125 TC21. *Mol Cell Biol* 21:3750-3762.
- 1126 Sanchez I, Hassinger L, Paskevich PA, Shine HD, Nixon RA (1996) Oligodendroglia
 1127 regulate the regional expansion of axon caliber and local accumulation of
 1128 neurofilaments during development independently of myelin formation. *J*
 1129 *Neurosci* 16:5095-5105.
- 1130 Savvaki M, Panagiotaropoulos T, Stamatakis A, Sargiannidou I, Karatzioula P,
 1131 Watanabe K, Stylianopoulou F, Karagogeos D, Kleopa KA (2008) Impairment
 1132 of learning and memory in TAG-1 deficient mice associated with shorter CNS
 1133 internodes and disrupted juxtaparanodes. *Mol Cell Neurosci* 39:478-490.
- 1134 Schneider S, Gruart A, Grade S, Zhang Y, Kroger S, Kirchhoff F, Eichele G, Delgado
 1135 Garcia JM, Dimou L (2016) Decrease in newly generated oligodendrocytes
 1136 leads to motor dysfunctions and changed myelin structures that can be rescued
 1137 by transplanted cells. *Glia* 64:2201-2218.
- 1138 Sommer I, Schachner M (1981) Monoclonal antibodies (O1 to O4) to oligodendrocyte
 1139 cell surfaces: an immunocytological study in the central nervous system. *Dev*
 1140 *Biol* 83:311-327.
- 1141 Spassky N, de Castro F, Le Bras B, Heydon K, Queraud-LeSaux F, Bloch-Gallego E,
 1142 Chedotal A, Zalc B, Thomas JL (2002) Directional guidance of oligodendroglial
 1143 migration by class 3 semaphorins and netrin-1. *J Neurosci* 22:5992-6004.
- 1144 Sun P, Watanabe H, Takano K, Yokoyama T, Fujisawa J, Endo T (2006) Sustained
 1145 activation of M-Ras induced by nerve growth factor is essential for neuronal
 1146 differentiation of PC12 cells. *Genes Cells* 11:1097-1113.
- 1147 Suter U, Scherer SS (2003) Disease mechanisms in inherited neuropathies. *Nat Rev*
 1148 *Neurosci* 4:714-726.
- 1149 Tanaka H, Ma J, Tanaka KF, Takao K, Komada M, Tanda K, Suzuki A, Ishibashi T,
 1150 Baba H, Isa T, Shigemoto R, Ono K, Miyakawa T, Ikenaka K (2009) Mice with
 1151 altered myelin proteolipid protein gene expression display cognitive deficits
 1152 accompanied by abnormal neuron-glia interactions and decreased conduction
 1153 velocities. *J Neurosci* 29:8363-8371.
- 1154 Tyler WA, Gangoli N, Gokina P, Kim HA, Covey M, Levison SW, Wood TL (2009)
 1155 Activation of the mammalian target of rapamycin (mTOR) is essential for
 1156 oligodendrocyte differentiation. *J Neurosci* 29:6367-6378.
- 1157 Wahl SE, McLane LE, Bercury KK, Macklin WB, Wood TL (2014) Mammalian target
 1158 of rapamycin promotes oligodendrocyte differentiation, initiation and extent of
 1159 CNS myelination. *J Neurosci* 34:4453-4465.
- 1160 Waxman SG (1980) Determinants of conduction velocity in myelinated nerve fibers.
 1161 *Muscle Nerve* 3:141-150.
- 1162 Waxman SG (1997) Axon-glia interactions: building a smart nerve fiber. *Curr Biol*
 1163 7:R406-410.
- 1164 Wiggins RC, Fuller GN, Dafny N (1982) Propagation of photic evoked responses
 1165 recorded from the retina, optic chiasm, lateral geniculate body, and visual cortex
 1166 of the nutritionally rehabilitated rat visual system. *Exp Neurol* 77:644-653.

- 1167 Wolswijk G (1998) Chronic stage multiple sclerosis lesions contain a relatively
1168 quiescent population of oligodendrocyte precursor cells. *J Neurosci* 18:601-609.
- 1169 Woodruff RH, Tekki-Kessaris N, Stiles CD, Rowitch DH, Richardson WD (2001)
1170 Oligodendrocyte development in the spinal cord and telencephalon: common
1171 themes and new perspectives. *Int J Dev Neurosci* 19:379-385.
- 1172 Zimmermann DR, Dours-Zimmermann MT (2008) Extracellular matrix of the central
1173 nervous system: from neglect to challenge. *Histochem Cell Biol* 130:635-653.
- 1174 Zuchero JB, Fu MM, Sloan SA, Ibrahim A, Olson A, Zaremba A, Dugas JC, Wienbar S,
1175 Caprariello AV, Kantor C, Leonoudakis D, Lariosa-Willingham K, Kronenberg
1176 G, Gertz K, Soderling SH, Miller RH, Barres BA (2015) CNS myelin wrapping
1177 is driven by actin disassembly. *Dev Cell* 34:152-167.
1178
1179

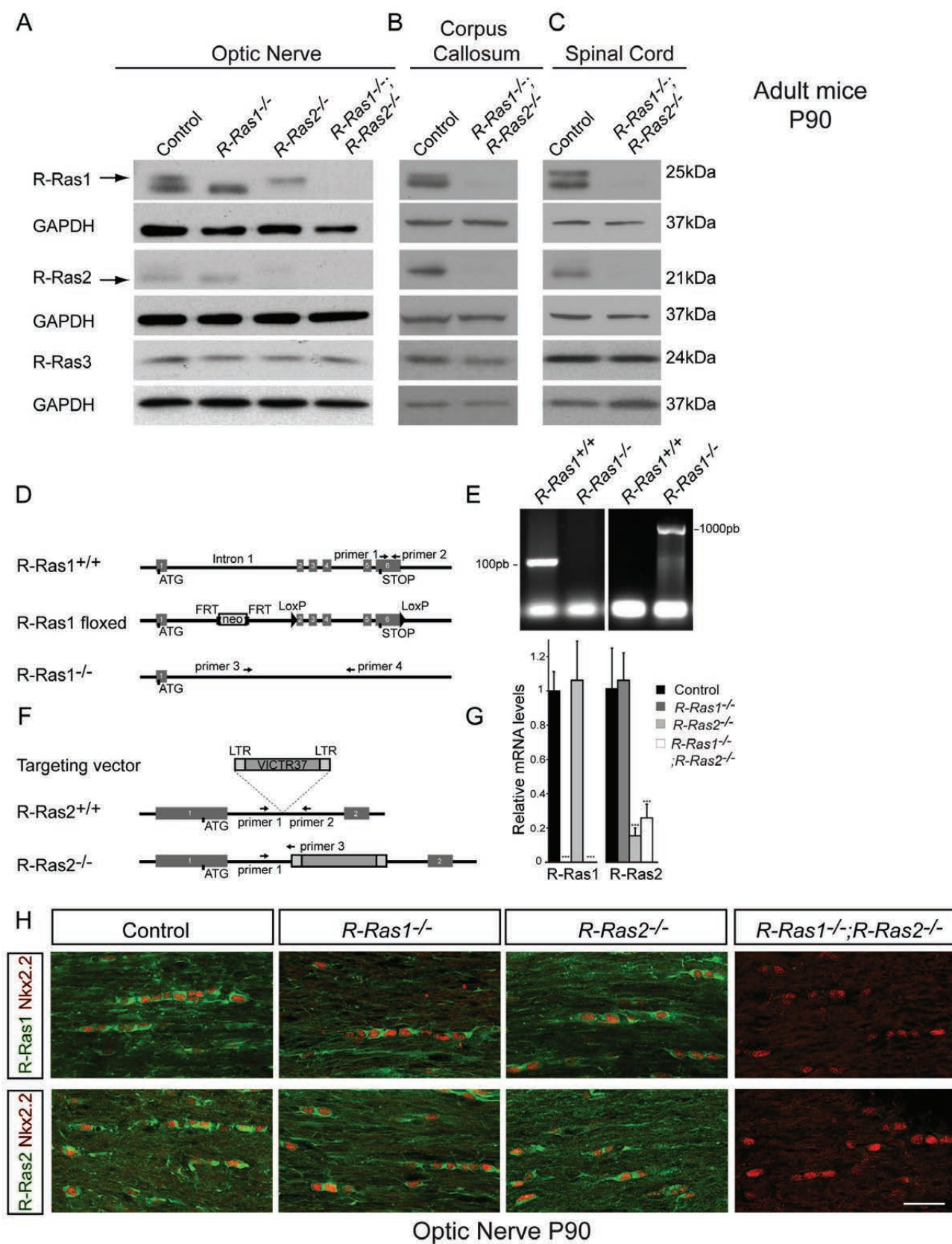


Figure 1

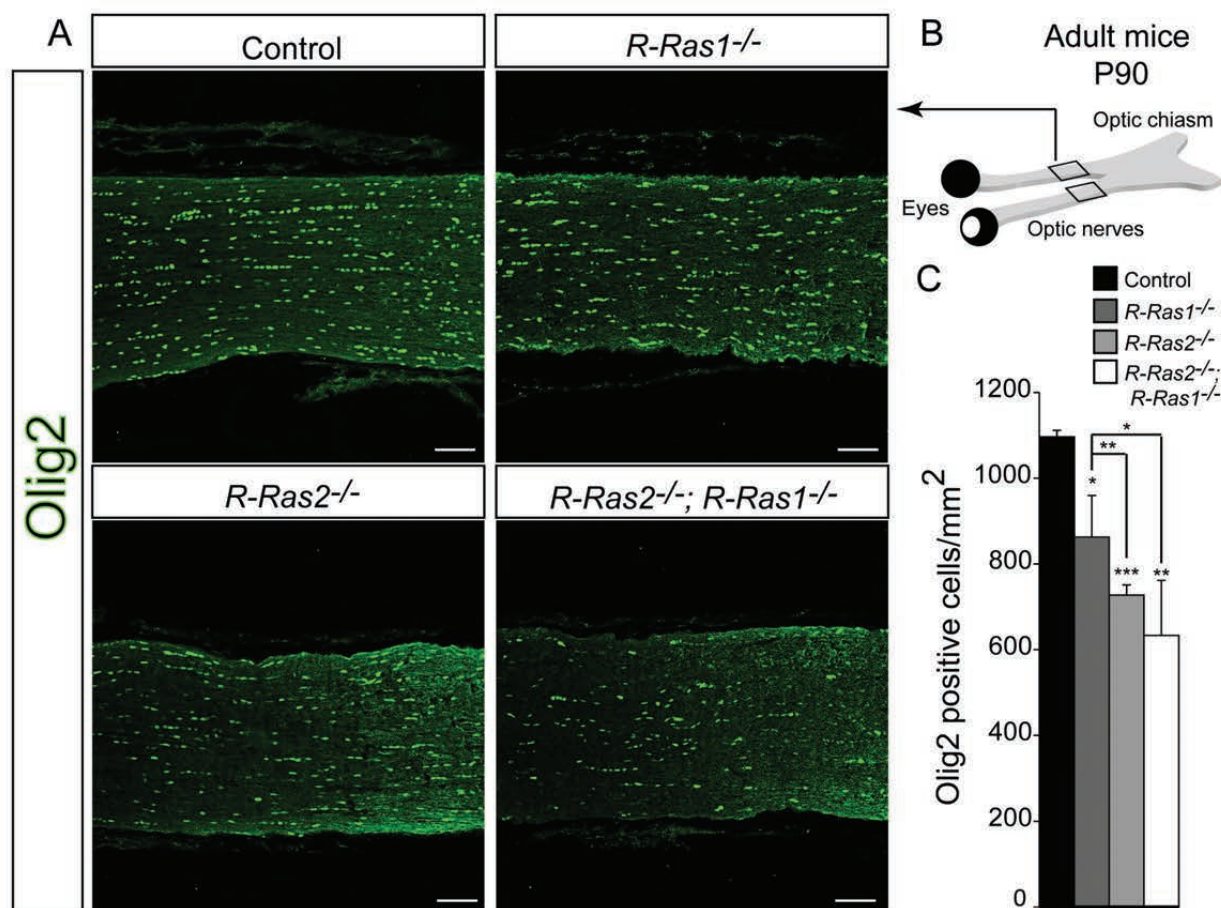


Figure 2

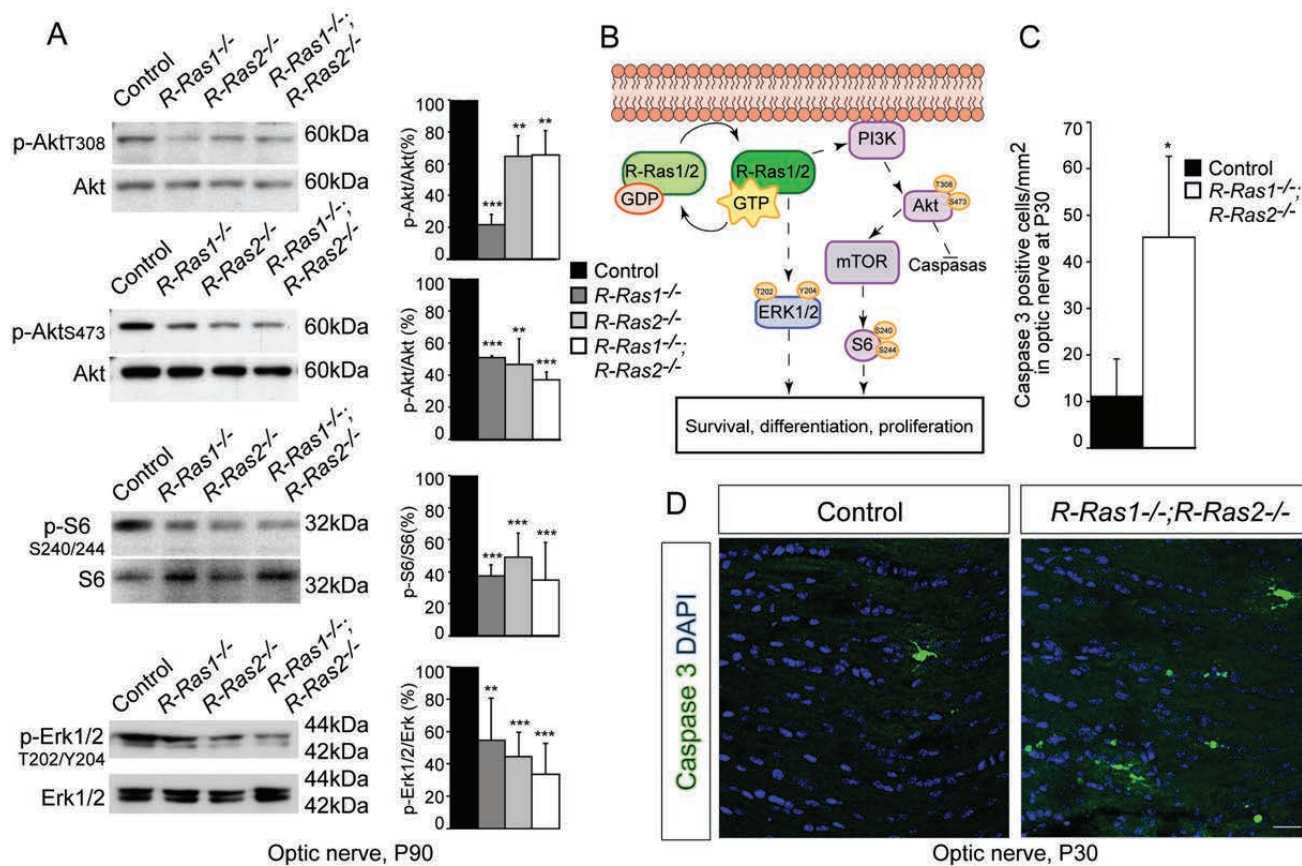


Figure 3

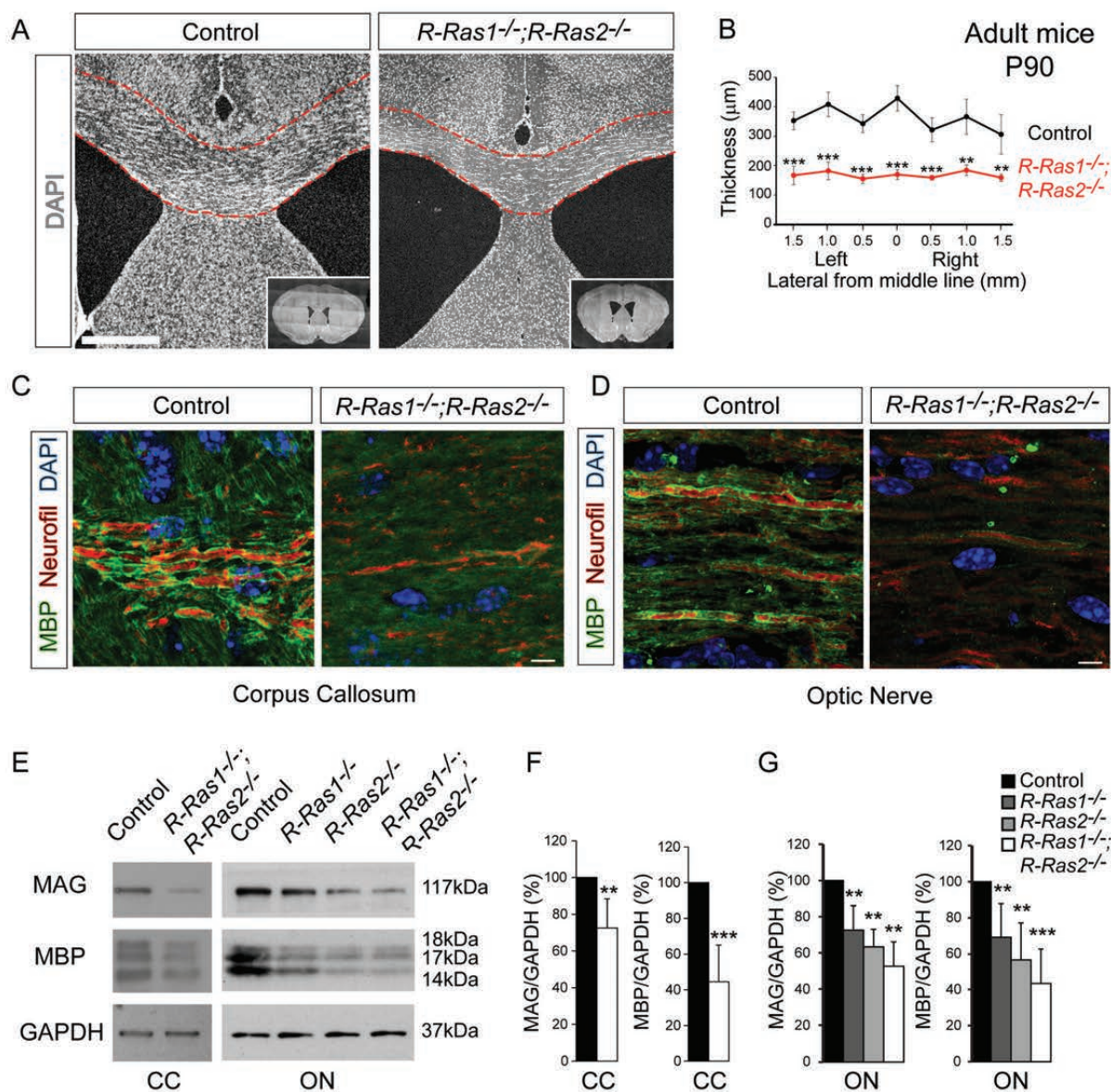


Figure 4

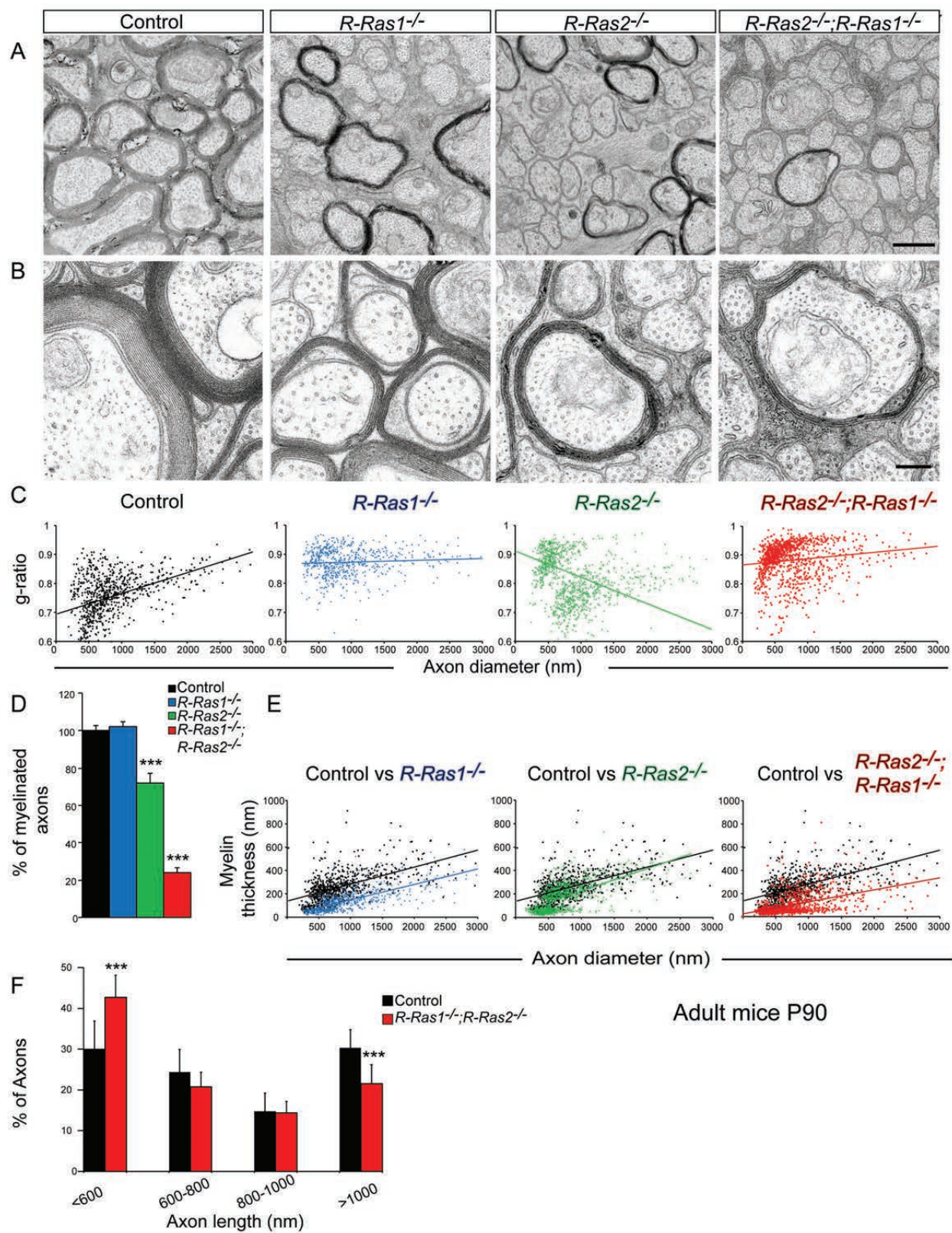


Figure 5

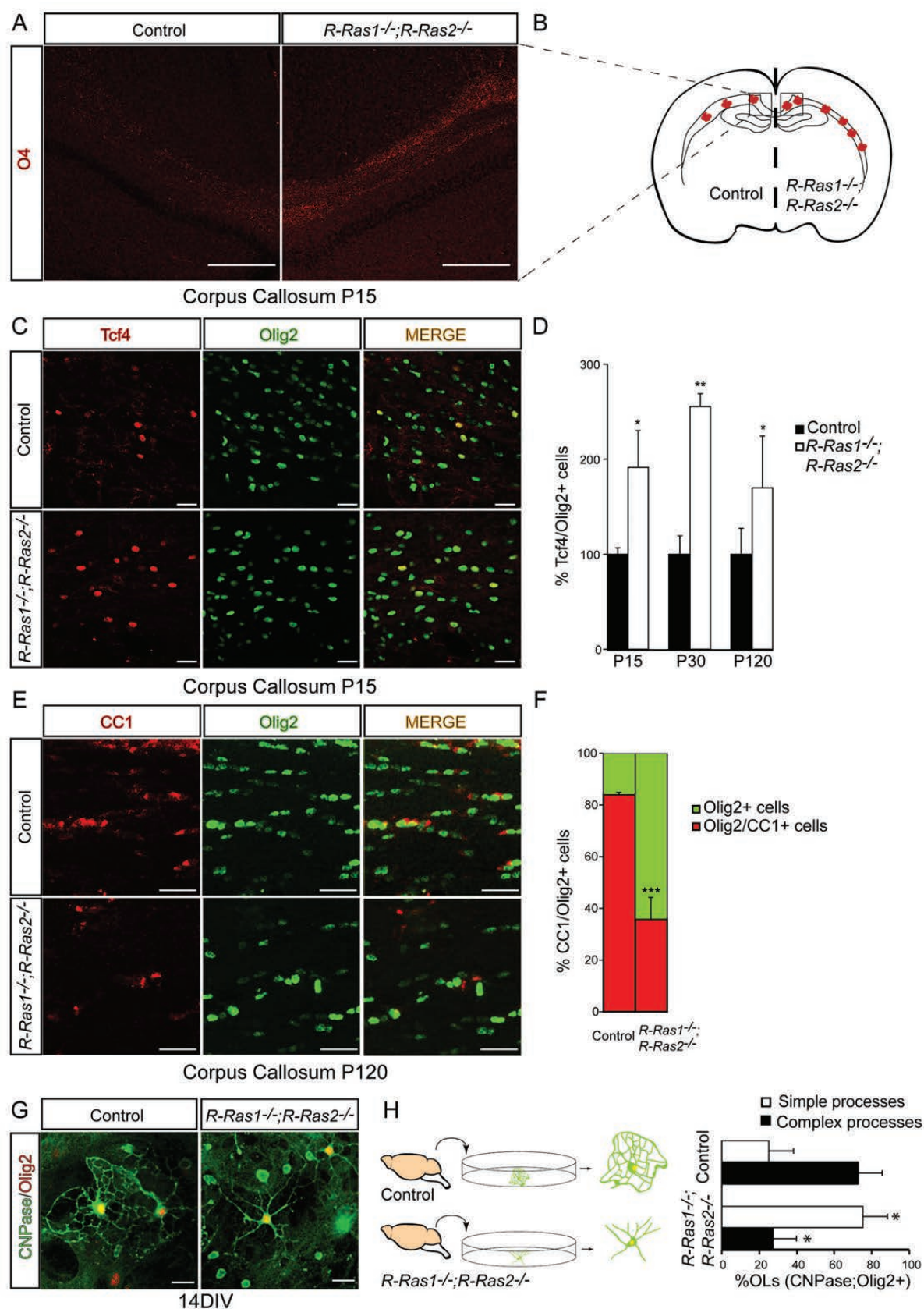


Figure 6

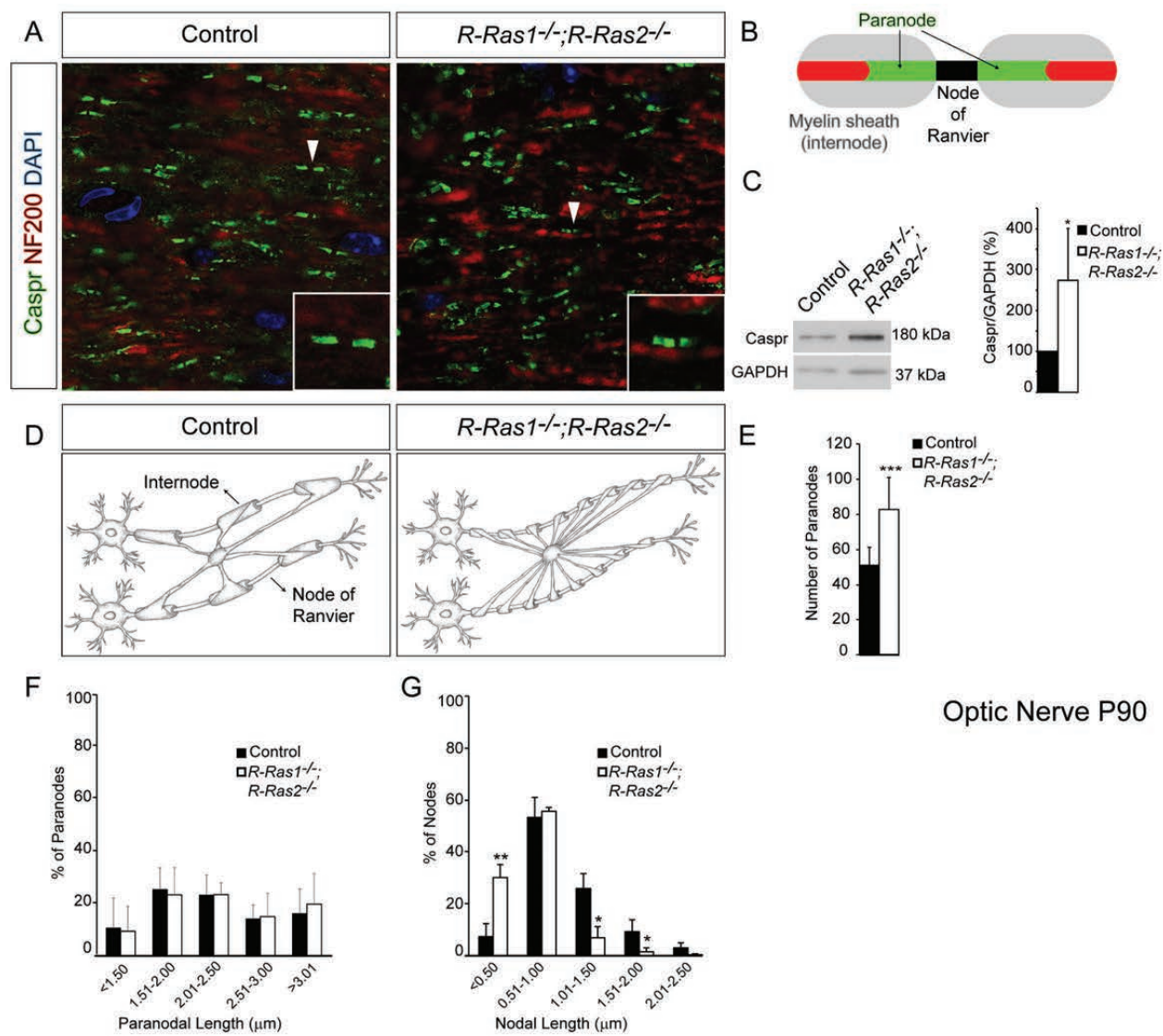


Figure 7

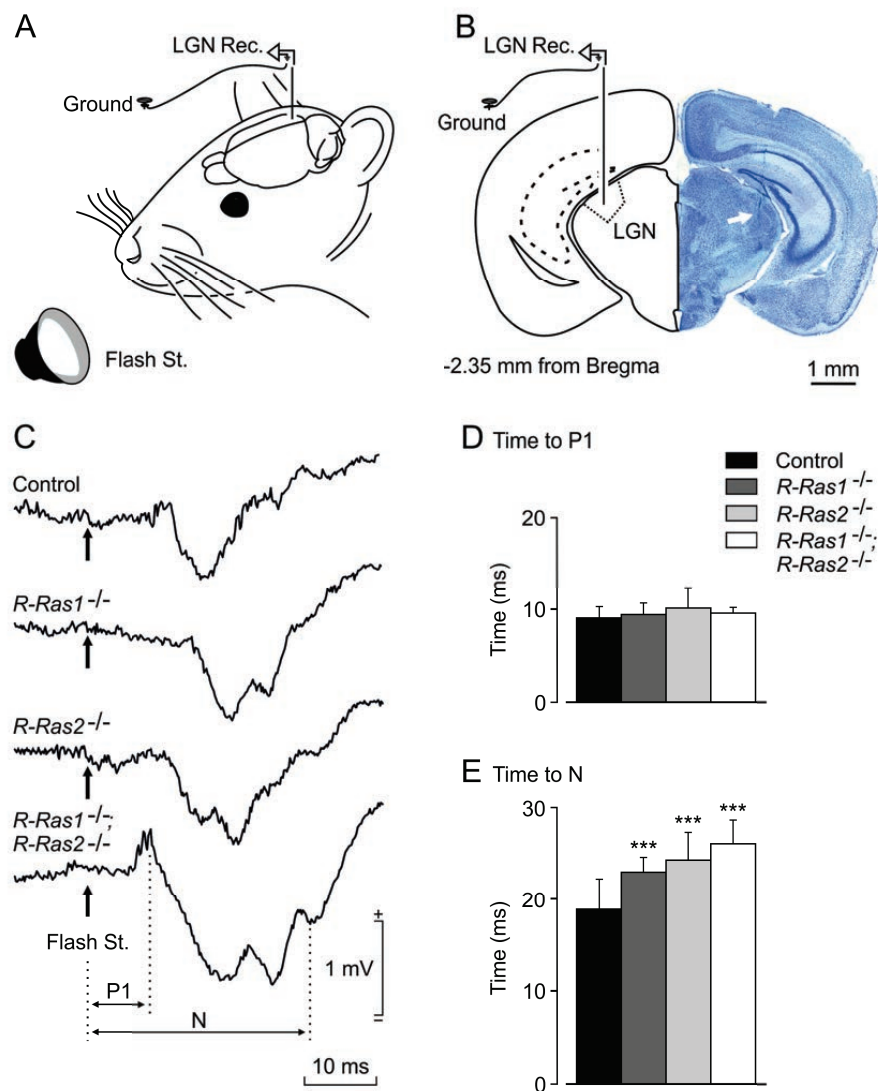


Figure 8